Universitatea
Transilvania
din Brașov

ȘCOALA DOCTORALĂ INTERDISCIPLINARĂ

Facultatea: Inginerie Electrică și Știința Calculatoarelor

Ing. Cosmin-Andrei HATFALUDI

Diagnostificarea bolilor vasculare, valvulare și inflamatorii ale inimii folosind rețele neurale adânci

Diagnosis of vascular, valvular and inflammatory cardiac diseases using deep neural networks

REZUMAT / ABSTRACT

Conducător științific

Prof.dr.ing. Lucian-Mihai ITU

BRAȘOV, 2024

Universitatea
Transilvania
din Brașov

D-lui (D-nei) .....

Componența

Comisiei de doctorat

Numită prin ordinul Rectorului Universității Transilvania din Brașov

Nr. ..... din .....

PREȘEDINTE:	- Prof. dr. ing. MORARU Sorin Aurel Director de departament Universitatea Transilvania din Brașov
CONDUCĂTOR ȘTIINȚIFIC:	- Prof. dr. ing. ITU Lucian Mihai Universitatea Transilvania din Brașov
REFERENȚI:	- Prof. dr. ing. MICLEA Liviu Cristian Universitatea Tehnică din Cluj Napoca
	- Prof. dr. ing. NECOARĂ Ion Referent Oficial, Universitatea Națională de Știință și Tehnologie Politehnica București
	- Prof. dr. fiz. URSUȚIU Doru Universitatea Transilvania din Brașov

Data, ora şi locul susținerii publice a tezei de doctorat: ....., ora ....., sala .....

Eventualele aprecieri sau observații asupra conținutului lucrării vor fi transmise electronic, în timp util, pe adresa cosmin.hatfaludi@unitbv.ro

Totodată, vă invităm să luați parte la şedința publică de susținere a tezei de doctorat.

Vă mulțumim.

Contents

1. Introduction

1.1 Introduction

Cardiac diseases persist as a primary contributor to global morbidity and mortality, highlighting the imperative for precise and prompt diagnosis. Recent advancements in medical imaging and computational methodologies have facilitated significant improvements in the accuracy of diagnostics and the quality of patient care. Deep Neural Networks (DNNs), in particular, have been at the forefront of this technological progress, showcasing exceptional proficiency in the analysis of intricate medical datasets. This paper delves into the utilization of DNNs for the diagnosis of vascular, valvular, and inflammatory cardiac conditions, specifically concentrating on coronary artery disease, aortic stenosis, and myocarditis. Through the adoption of deep learning techniques, researchers and healthcare professionals are able to detect nuanced patterns within medical imagery that traditional methods might overlook, thus paving the way for advancements in cardiac care that are both more precise and personalized.

1.2 Deep Neural Networks in Cardiac Diagnosis

Deep learning techniques empower computational models to learn data representations through multiple processing layers, enabling them to abstract information at different levels [1]. At the heart of these deep learning methods are Artificial Neural Networks (ANNs), which are essential for their operation. ANNs are comprised of numerous artificial neurons, as illustrated by a basic example in Figure 1.1.

Within an ANN, each artificial neuron processes multiple inputs into a single output. These inputs are individually weighted, summed, and often adjusted by an additional bias term before being processed through a nonlinear function. The capability of ANNs to layer multiple neurons enables the modeling of complex nonlinear input-output relationships, crucial for generating precise predictions. As we can see in Figure 1, the ANN takes as input some characteristics about the patient and learns to predict the 10 year cardiovascular risk. Despite their origins in the late 1950s [1] and early applications in medical imaging by 1995 [2], ANNs did not gain their current popularity until recently. This shift is largely attributed to both methodological advancements and the increased availability of computational resources, overcoming previous limitations of shallow network architectures that could not effectively model the intricate relationships in medical images. Nowadays, with the advent of more accessible computational power, researchers are developing ANNs with dozens or even hun-

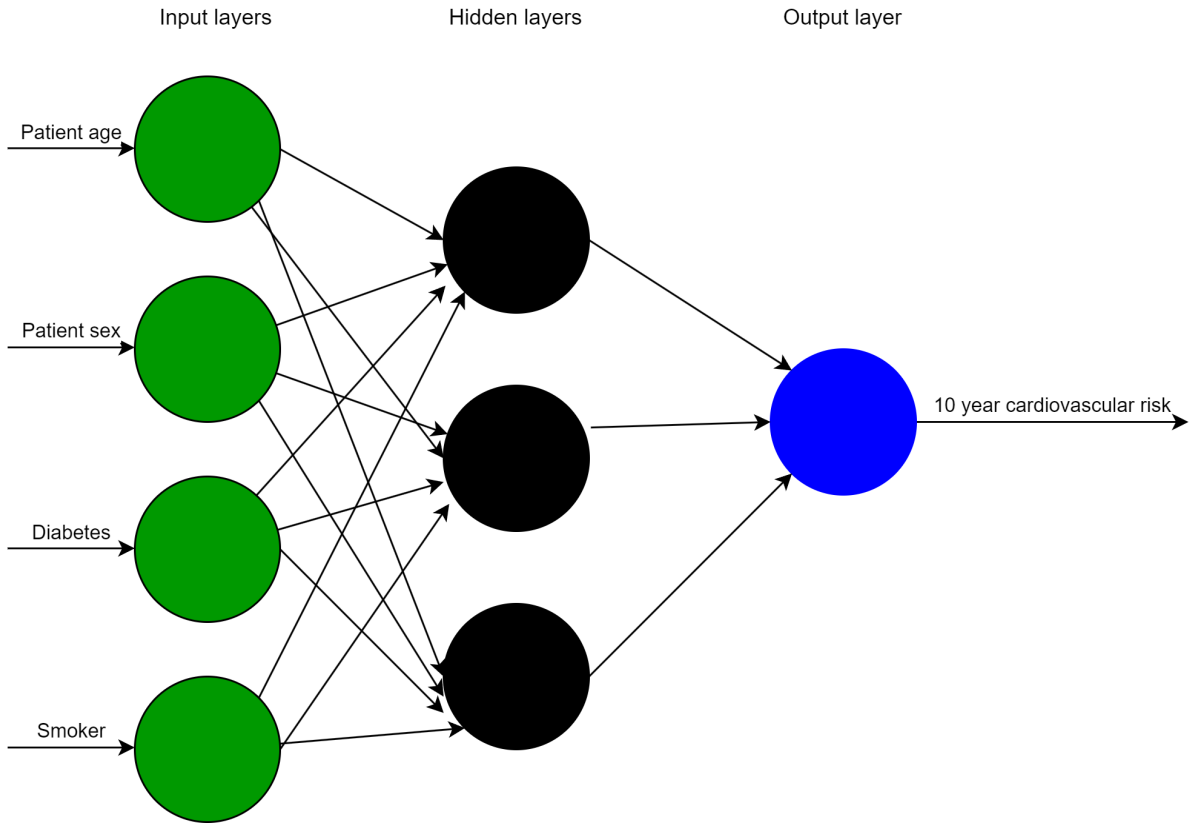

Figure 1.1: Illustration of an ANN that predicts the 10 year cardiovascular risk.

dreds of layers, facilitating the direct analysis of medical images without the need for prior feature extraction.

The selection of a neural network's architecture is determined by the specific problem it is designed to solve. The term "architecture" in this context refers to the configuration of the neural network, including the number and arrangement of layers and neurons, as well as their interconnections. For tasks in image analysis, Convolutional Neural Networks [3] (CNNs) are frequently the architecture of choice. Unlike traditional ANNs, CNNs significantly reduce the quantity of parameters (weights) by employing shared weights across different locations in the image. This reduction is achieved through the application of convolution operations, thereby earning the designation "convolutional" neural network. An example of a convolution neural network applied on a medical image is depicted Figure 1.2. CNN architectures typically incorporate both convolutional layers and pooling layers. Pooling layers, which do not possess weights, serve to downsample the input data, often by a factor of 2, decreasing the image's resolution but enlarging the field of view for the layers that follow. This enlargement is instrumental for CNNs in integrating greater contextual information from images. For tasks such as image classification or regression, convolutional networks often conclude with fully connected layers, which resemble those found in standard ANNs and aim to consolidate the extracted feature information into a singular predictive output. In applications requiring image segmentation, such as segmenting the left or right ventricle in cardiovascular imaging, CNN architectures can be specially tailored. These specialized architectures, capable of accepting an image as input and directly producing a segmented output at the image scale, are referred to as Fully Convolutional Networks (FCNs). One FCN network architecture is known as U-Net, with many applications in medical imaging [4].

Another neural network architecture employed in medical imaging is the Recurrent Neural Network (RNN) [5]. RNNs utilize a feedback loop mechanism, enabling the network to retain information from previous inputs and incorporate it into the processing of future sequences, thereby creating a

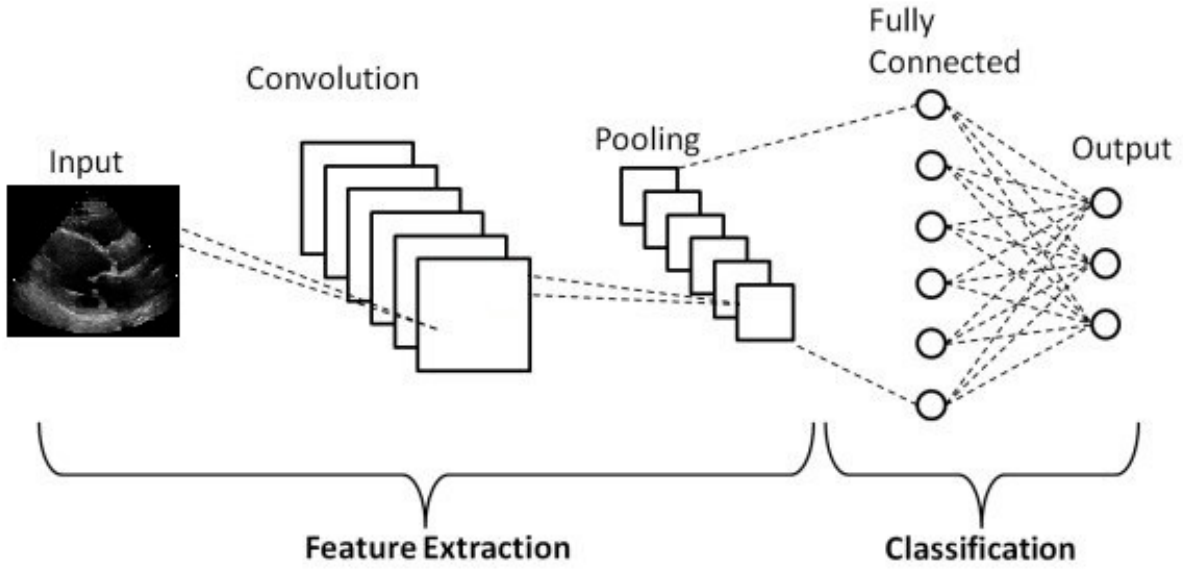

Figure 1.2: Simple illustration of a CNN.

memory effect that is essential for processing sequential data, including applications in electrocardiography, textual analysis, or cine-MRI studies. An RNN operates by processing the initial element of a sequence to generate a prediction, then iteratively combines its previous output with the subsequent sequence element for future predictions, as illustrated in Figure 1.3. RNNs represent a class of sophisticated dynamic models capable of handling temporal dependencies; however, their training poses significant challenges. The difficulty arises from the phenomenon where gradients propagated back through the network during training either increase or decrease exponentially with each time step. As a result, across numerous steps, these gradients tend to either explode or vanish [6], complicating the network's effective training.

Building on the discussion of neural network architectures such as ANNs, CNNs, RNNs, it is essential to delve into their deployment within the medical diagnosis and imaging context, framed by supervised and unsupervised learning paradigms [7]. In the realm of supervised learning, these neural networks are trained with labeled medical datasets, where each input (e.g., an MRI image) is associated with a specific diagnosis or outcome. This method is particularly valuable for diagnostic tasks, where precise predictions—such as identifying the presence of tumors or classifying different stages of a disease—are critical. Supervised learning enables these networks to learn from historical, annotated medical data, enhancing their accuracy in diagnosing new cases. In contrast, unsupervised learning allows neural networks to analyze medical images without predefined labels, offering a powerful tool for discovering novel patterns or anomalies that may not have been previously known. This approach is beneficial for segmenting complex medical images, identifying patient groupings based on disease markers, or even uncovering new diagnostic indicators within medical data. Unsupervised learning in medical imaging can lead to the development of new diagnostic criteria and the exploration of uncharted territories in patient data, facilitating a deeper understanding of diseasess Both learning paradigms significantly contribute to advancing medical diagnosis and imaging, tailoring neural network architectures to meet the specific needs of medical professionals and researchers. By leveraging supervised learning, neural networks can achieve high precision in diagnostic tasks, while unsupervised learning offers the potential for breakthrough discoveries in understanding and classifying diseases, showcasing the versatile application of these technologies in enhancing patient care and medical research.

In this section, we present a comprehensive overview of the latest advancements in utilizing deep learning algorithms for cardiovascular imaging. The discussion is structured by imaging modality, with a primary focus on ultrasound, CT, and MRI, while also covering other modalities in a collective

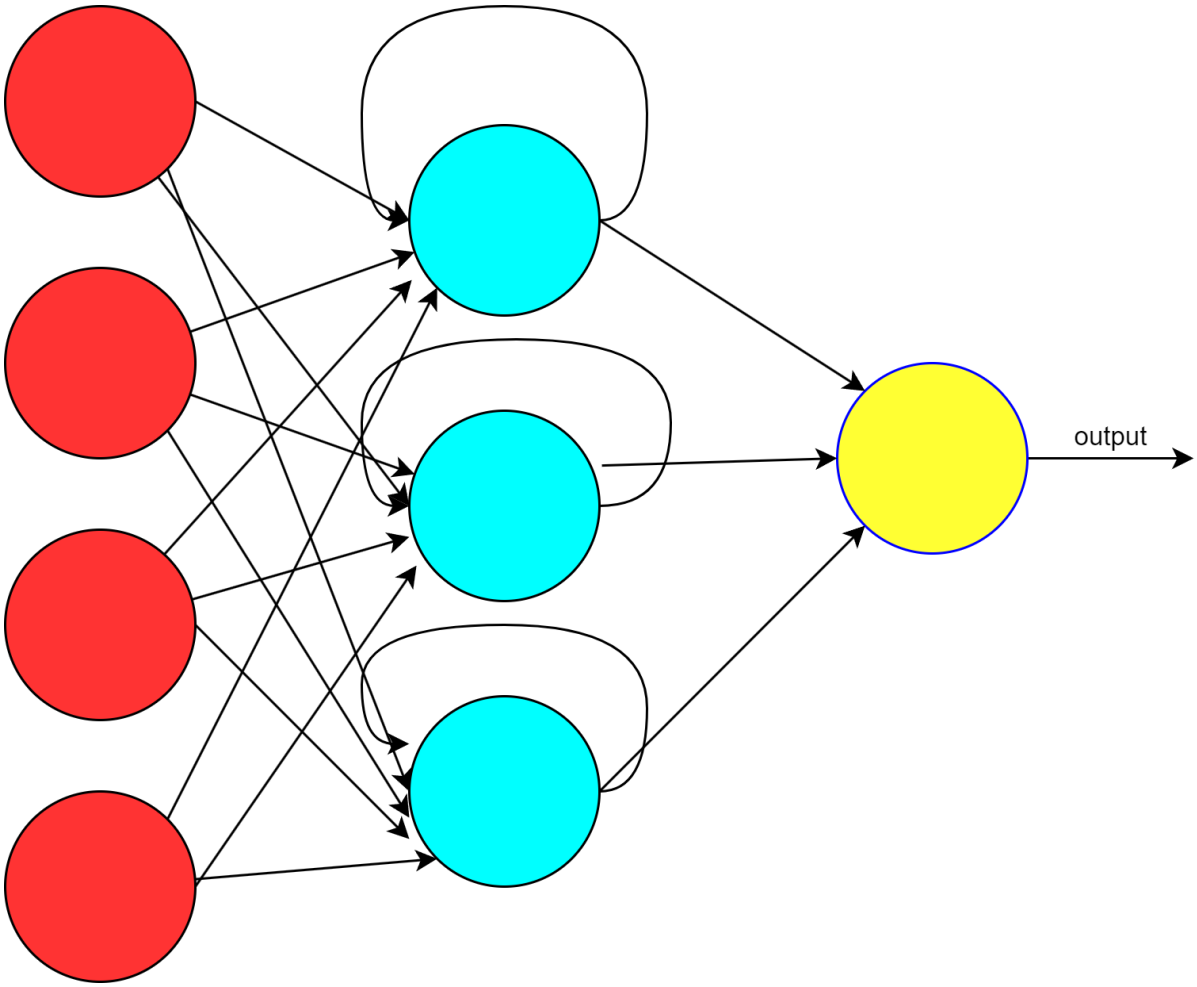

Figure 1.3: Simple illustration of a RNN network. The curved arrows highlight the feedback loop of RNNs.

manner.

Deep learning has made significant strides in the field of cardiovascular ultrasound, with applications spanning detection, classification, segmentation, tracking, and the generation of reports. Moradi et al. [8] pioneered a technique that leverages a deep learning model to understand the relationship between electronic medical records and echocardiography images, facilitating the selection of pertinent medical records for specific echocardiography images. In work by Chen et al. [9], a Convolutional Neural Network (CNN) was employed to accurately segment the left ventricle from five distinct 2D perspectives, demonstrating the superior segmentation capabilities of multiview CNNs. Carneiro et al. [10] first applied an Artificial Neural Network (ANN) to predict landmarks critical for outlining the left ventricle's segmentation contour. This method was later expanded to include left ventricle tracking and enhanced through the integration with multi-atlas registration techniques for refined segmentation. Dong et al. [11] and Ghesu et al. [12] have successfully combined deep learning with conventional techniques for segmenting the left ventricle and aortic valve, respectively, with the approach by Ghesu et al. [12] achieving a segmentation quality improvement of over 40% compared to previous methodologies. The task of disease classification using echocardiography has been investigated by Diller et al. [13], Jun et al. [14], and Zhang et al. [15], with the study by Zhang et al. [15] reporting strong classification performance utilizing a comprehensive dataset comprising more than 14,000 echocardiograms. Additionally, deep learning has proven effective for the classification of time points and views in ultrasound sequences, as evidenced by the methodologies developed by Dezaki et al. [16] and Abdi et al. [17] for identifying end systolic and end diastolic frames, and

evaluating the quality of echo series, respectively.

In the realm of CT imaging, deep learning techniques are employed for a variety of critical tasks, including the localization and segmentation of anatomical features, serving vital clinical needs in both noncontrast CT scans and coronary CT angiography (CCTA). Commandeur et al. [18] successfully applied Convolutional Neural Networks (CNNs) to delineate epicardial and thoracic adipose tissue in noncontrast cardiac CT images, delivering precise segmentation across a broad patient base. Zreik et al. [19] introduced a multiscale, patch-based CNN approach for segmenting the left ventricular myocardium, proving its effectiveness in the accurate quantification of volumes. Wu et al. [20] leveraged a Long Short-Term Memory (LSTM) Recurrent Neural Network (RNN) for the task of segment labeling within the coronary artery tree, opening new avenues for the identification of plaque and stenosis. Furthermore, the role of deep learning extends to the detection of atherosclerosis in noncontrast CT scans, with studies by Wolterink et al. [21] and Lessmann et al. [22] showcasing the successful identification of coronary artery and aortic calcifications through CNN-based strategies.

Deep learning's application to MRI has been predominantly centered on segmentation tasks, especially concerning cardiac structures to evaluate cardiac function, with contemporary methods reaching the accuracy level of human experts [23]. Before the advent of deep learning, segmentation relied heavily on techniques such as multi-atlas registration and deformable shape models. Initial forays sought to combine deep learning with these traditional methods [24, 25, 26, 27]. However, the focus has shifted towards leveraging Convolutional Neural Networks (CNNs) in recent advancements [28]. Bernard et al. [28] conducted a review of cardiac MRI analysis techniques, finding widespread use of CNNs for automatic segmentation and the classification of pathologies, marking a significant evolution in the field. Innovations include the adoption of both 2D and 3D U-nets for enhanced segmentation accuracy [29]. Vigneault et al. [29] contributed to this progress by improving the segmentation of the left and right ventricular cavities. The Kaggle Data Science Bowl in 2015 [30] motivated a surge in segmentation-focused methods aimed at evaluating the left ventricular ejection fraction (LVEF) [31, 32, 33]. Beyond segmentation, deep learning's utility in cardiovascular MRI also covers scar tissue identification [34, 35, 36], quality assessment, precise localization, and image reconstruction [37, 38, 39, 40, 41], offering a quicker and more practical solution compared to traditional manual tracing of cardiac structures [42]. Deep learning has also shown promise in pinpointing specific time frames within cardiac cine-MRI and in MRI imaging without the need for breath-holding [39, 40], and it has demonstrated superiority over compressed sensing techniques in reconstructing dynamic cardiac MRI images [41].

Deep learning's impact extends beyond traditional imaging modalities, as evidenced by pioneering efforts in nuclear cardiology by Betancur et al. [43, 44], who leveraged Convolutional Neural Networks (CNNs) for the diagnosis of obstructive diseases through myocardial perfusion imaging using single-photon emission computed tomography, analyzing a large dataset of over 1,600 patients from multiple medical centers. This innovation in nuclear cardiology is part of a broader application of deep learning across various imaging techniques. In the domain of intraoperative x-ray imaging, deep learning enhances functionality through real-time image denoising [45], accurate stent segmentation [46], and the synchronization of preoperative cardiac models with intraoperative x-ray fluoroscopy [47]. Similarly, in intravascular optical coherence tomography, CNNs are instrumental for plaque detection and classification [48, 49, 50], vessel lumen segmentation for stenosis assessment [51], and the derivation of heart motion from intraoperative videos [52]. These advancements underscore deep learning's transformative potential in improving diagnostic accuracy, procedural planning, and execution across multiple modalities, including nuclear cardiology and intraoperative imaging techniques. Together, these applications illustrate the versatility and comprehensive utility of deep learning in enhancing the diagnosis and treatment planning in a wide array of clinical settings, bridging the gap between various imaging modalities and paving the way for integrated, precision-driven healthcare solutions.

1.3 Vascular Diseases

Vascular disorders represent a diverse array of conditions that impair the function and structure of blood vessels, including arteries, veins, and lymphatics, leading to substantial global health care challenges due to their widespread prevalence and the significant morbidity and mortality they cause [53]. These pathologies interfere with the vessels' capacity to efficiently circulate blood throughout the organism, encompassing a range from arterial obstruction due to atherosclerotic plaque formation to venous thromboembolic incidents and inflammation-induced vasculitis. Among these, Peripheral Artery Disease (PAD) emerges when atherosclerotic plaques accumulate in the peripheral arteries, eliciting claudication and ischemic manifestations in the lower extremities. Carotid artery disease, characterized by stenosis of the carotid arteries, escalates the risk for cerebrovascular accidents. Venous conditions such as varicose veins and Deep Vein Thrombosis (DVT) originate from venous incompetence and thrombotic episodes. Aortic aneurysms, inclusive of both thoracic and abdominal variants, represent significant rupture hazards. Vasculitis denotes the inflammatory alterations within the vessel walls, impacting diverse organs and tissues.

The diagnostic process for vascular diseases incorporates clinical evaluations alongside imaging methodologies. Non-invasive imaging techniques like ultrasound facilitate the immediate observation of hemodynamics and vascular structure. Conversely, invasive diagnostic approaches such as catheter angiography are indispensable for detailed arterial examination. Advanced imaging technologies, including Computed Tomography (CT) and Magnetic Resonance (MR) Angiography, provide intricate anatomical insights.

The etiology of vascular diseases is multifactorial, with modifiable risk elements like tobacco use, dyslipidemia, hypertension, and diabetes mellitus playing a significant role. Conversely, non-modifiable determinants such as genetic factors and chronological aging also influence susceptibility to these disorders.

Therapeutic interventions for vascular diseases prioritize lifestyle alterations, pharmacologic treatment, and surgical or endovascular techniques. Lifestyle modifications, including cessation of smoking and adoption of regular physical activity, are fundamental in managing risk factors. Pharmacotherapies aimed at modulating lipid metabolism and inhibiting platelet aggregation contribute to slowing disease progression. Meanwhile, invasive remedies, such as angioplasty and the insertion of stents, prove efficacious in re-establishing perfusion in obstructed conduits.

1.3.1 Coronary Artery Disease

Cardiovascular disease (CVD) continues to be the primary global cause of death and disability, largely attributed to atherosclerosis, an inflammatory condition that leads to arterial obstruction and frequently progresses to coronary artery disease (CAD) [54, 55]. Despite the established predictive value of traditional risk factors such as age, sex, and diabetes [56], along with genetic predispositions [57], the prediction of clinical outcomes like ischemic tissue damage remains challenging when relying solely on these indicators [58, 59, 60].

The development of coronary collateral circulation (CCC), characterized by the formation of natural bypass routes or collateral arteries, is crucial in alleviating ischemic tissue damage and enhancing survival rates [61, 62, 63, 64, 65]. Yet, the detection methods for CCC have not kept pace with its clinical significance. To address this issue, we propose an innovative technique employing deep neural networks to identify CCC from invasive coronary angiography (ICA) images, the gold standard for diagnosing CAD [66].

Previous efforts to detect CCC from ICA have been scarce, with related research focusing on the assessment of collateral physiology under conditions of total occlusion [66], vessel segmentation for collateral scoring in brain CT angiography [67], and the development of automated collateral scoring algorithms [68]. Furthermore, deep learning has been applied to evaluate collaterals in patients with ischemic stroke using CT angiography [69], although the dynamic nature of coronary vessels during cardiac cycles poses a significant challenge for CCC detection [69].

Deep learning techniques have also been extensively applied in analyzing ICA and CTA images for a variety of cardiovascular applications, including coronary artery segmentation [70], calcium scoring [71], and predicting cardiovascular hemodynamics for bypass surgery planning [72].

1.4 Valvular Diseases

Valvular heart disease encompasses a spectrum of pathologies affecting the cardiac valves, compromising their function [73]. The human heart consists of four chambers and an equal number of valves: the mitral, tricuspid, aortic, and pulmonary valves, which play a pivotal role in regulating hemodynamics [74].

The array of conditions classified under valvular heart disease includes regurgitation, stenosis, and atresia. Regurgitation is defined by the inability of a valve to close completely, resulting in the backward flow of blood. Stenosis refers to the narrowing of a valve orifice, impeding the forward flow of blood, whereas atresia describes a complete absence of a valve opening. Any of the cardiac valves may be afflicted by these disorders, affecting the overall efficiency of the cardiovascular system.

The etiology of valvular heart disease is varied, ranging from congenital anomalies and infectious agents such as endocarditis, to degenerative modifications associated with aging, and complications of other cardiovascular diseases including heart failure and atherosclerosis. Rheumatic heart disease, a sequelae of rheumatic fever following streptococcal infections, remains a significant global health issue, albeit its prevalence has diminished in areas with accessible antibiotic therapy.

Clinical manifestations of valvular heart disease are diverse and may include dyspnea, thoracic discomfort, fatigue, vertigo, arrhythmias, and edema resulting in sudden weight gain. Symptomatology and severity are highly variable, with some individuals remaining symptom-free until the disease progresses to an advanced stage.

The diagnostic evaluation of valvular heart disease frequently begins with auscultation to identify abnormal cardiac sounds or murmurs. Echocardiography stands as a cornerstone in the diagnostic imaging of these conditions, offering detailed insights into valve morphology and functionality.

The therapeutic management of valvular heart disease is multifaceted, typically involving pharmacological treatment alongside surgical intervention. Medications aim to mitigate symptoms and manage concurrent conditions such as hypertension. Nonetheless, in severe cases, surgical correction or valve replacement becomes imperative. The choice between traditional open-heart surgery and less invasive surgical options is contingent upon the specific valve involved and the patient's general health status.

1.4.1 Aortic Stenosis

Aortic stenosis (AS) is a common valvular heart disease observed in 2% to 5% of the elderly population, presenting significant clinical challenges amidst an aging demographic [75]. Echocardiography is the foremost non-invasive technique for evaluating AS and guiding therapeutic decisions [75]. The primary cause of AS is linked to degenerative changes, with current therapeutic strategies limited to aortic valve (AV) replacement due to the absence of medical treatments capable of decelerating the disease's progression [76]. Present guidelines for AV replacement are mainly based on the severity of the condition and patient symptoms, which may neglect essential factors like detailed lesion analysis [77]. Particularly, low flow and low gradient AS, which accounts for 35-40% of cases, introduces diagnostic dilemmas that could result in suboptimal therapeutic interventions, underscoring the necessity for refined diagnostic methodologies [78].

The integration of echocardiographic data with clinical insights into artificial intelligence (AI) frameworks appears promising for augmenting the precision of AS severity evaluations and therapeutic planning [79]. Nevertheless, the comprehensive evaluation of AS requires extensive echocardiographic measurements, leading to protracted examination times [79]. Recent research underscores the capacity of AI, especially deep learning (DL), to autonomously identify and quantify echocardio-

graphic indices [80, 81, 82, 83]. However, an automated or AI-driven method for a complete AS evaluation using echocardiography has yet to be established [84].

The exploitation of AI and advancements in DL methodologies have the potential to transform the diagnostic and therapeutic landscape of AS. Applying AI algorithms to automate the detection and analysis of echocardiographic metrics could significantly streamline diagnostic procedures and refine therapeutic decisions. Such progress promises to enhance patient care and optimize the allocation of healthcare resources in treating this widespread cardiovascular ailment.

1.5 Inflammatory Cardiac Diseases

Inflammatory cardiac diseases represent a group of pathologies characterized by inflammation within the heart, manifesting in conditions such as pericarditis, endocarditis, and myocarditis [85]. These diseases, though relatively uncommon, span a spectrum from mild to critical, necessitating individualized therapeutic strategies and potentially extended convalescence. The primary anatomical regions of the heart affected by these conditions include the endocardium, myocardium, and pericardium. Specifically, endocarditis is characterized by inflammation of the heart's inner lining, including its chambers and valves. Myocarditis involves inflammation of the cardiac muscle, adversely affecting its contractile function, while pericarditis is the inflammation of the enclosing pericardial sac.

Risk factors for these inflammatory cardiac conditions encompass a range of medical states such as diabetes and HIV/AIDS, alongside medical interventions like catheterization and exposure to radiation therapy. Common symptomatic presentations include thoracic pain, dyspnea, and pyrexia, with the specific clinical picture dependent on the inflammation's location. Infectious agents, notably viruses and bacteria, are the predominant causes, although autoimmune diseases, environmental exposures, and certain pharmacological agents may also precipitate cardiac inflammation. Potential complications arising from unaddressed inflammatory cardiac diseases include thromboembolic events, cardiac insufficiency, arrhythmias, and disseminated infections.

The diagnostic approach to these conditions is multifaceted, integrating physical assessments, review of patient history, and diagnostic imaging modalities such as cardiac computed tomography (CT), electrocardiogram (EKG), echocardiography, and magnetic resonance imaging (MRI). Therapeutic management is directed towards symptomatic relief, eradication of infection, and minimization of myocardial stress, employing agents like corticosteroids, antibiotics, and anti-inflammatory medications. In instances of severe disease, interventions may extend to pericardial effusion drainage or surgical procedures. Preventative measures focus on mitigating known risk factors, enhancing oral hygiene to diminish the risk of endocarditis, and seeking early medical consultation for indicative symptoms.

The prognosis and outlook for patients with inflammatory cardiac diseases are contingent upon the condition's severity and the promptness of medical intervention. While certain cases may resolve with conservative management or spontaneous remission, others may necessitate advanced treatment modalities, including ventricular assist devices or cardiac transplantation.

Management of life with inflammatory cardiac diseases demands compliance with pharmacological regimens, regular medical follow-ups, and immediate reporting of novel symptoms. Urgent medical care should be sought for new onset chest pain, indicative of potential severe cardiac complications.

1.5.1 Myocarditis

Myocarditis, defined by the inflammation of the myocardium, significantly impacts myocardial contractility and electrophysiological properties, with potential progression to heart failure and arrhythmogenic events [86]. Its etiology is complex, encompassing infectious etiologies such as viral infections (e.g., COVID-19, parvovirus), systemic inflammatory and autoimmune conditions, as well

as adverse reactions to medications [87]. The clinical presentation often includes chest pain, fatigue, and shortness of breath [88], underscoring the importance of early cardiological evaluation for prompt identification and intervention. In advanced cases, endomyocardial biopsy may be necessary for definitive diagnosis [89]. The therapeutic approach to myocarditis involves a combination of supportive care, management strategies for heart failure, targeted antimicrobial therapy against identified pathogens, and immunosuppressive treatments for pronounced inflammatory reactions. The importance of early detection and therapeutic initiation cannot be overstated in mitigating adverse outcomes. While cardiovascular magnetic resonance imaging (MRI) is instrumental in diagnosing myocarditis, its analysis requires substantial expertise, introducing potential for laborious processes and subjective interpretation [90]. To surmount these diagnostic challenges, there has been a push towards the development of automated diagnostic systems leveraging sophisticated machine learning algorithms to augment diagnostic precision and minimize interpretative variability [90]. Deep learning (DL), with its capacity for intricate feature discernment through multiple layers, presents a promising approach for myocarditis identification via cardiovascular MRI [91]. The adoption of Few-shot learning (FSL) techniques, which operate effectively with minimal data inputs, further bolsters diagnostic performance [8]. Recent innovations in DL applied to myocardial disease (MCD) diagnosis have shown notable advancements. For instance, Sharifrazi et al. [88] introduced a Convolutional Neural Network-Keras Custom Layer (CNN-KCL) model, attaining a remarkable 97.41% accuracy in MCD detection from cardiovascular MRI. Similarly, Shoeibi et al. [92] applied cycle-Generative Adversarial Network preprocessing and leveraged pre-trained models to achieve a 99.33% accuracy utilizing the EfficientNet V2 framework. Additionally, Moravvej et al. [93] investigated the application of deep reinforcement learning (RL) for MCD diagnosis, proposing the RLMD-PA method, which showed improved accuracy and efficiency.

1.6 Thesis Structure and Content

This thesis investigates the application of Deep Learning (DL) techniques across various domains of medical imaging, focusing specifically on the diagnosis of cardiac-related conditions (vascular, valvular and inflammatory cardiac diseases). The document is meticulously organized into six chapters, each serving a distinct purpose within the overarching theme of leveraging DL for medical diagnostics

The **first chapter** sets the stage with an introduction into cardiac diseases, emphasizing the prevalence and impact of vascular, valvular, and inflammatory conditions on global health. It then transitions into a discussion on the evolution of diagnostic techniques, charting the course from conventional methodologies to the cutting-edge advances brought about by DL technologies. This narrative not only highlights the technological strides but also underscores the potential of DL to revolutionize the diagnostic landscape by enhancing the precision and predictability of cardiac disease diagnosis. Moreover, this introduction outlines the thesis's core objective: to delve into the application of DL in medical imaging for cardiac diagnostics, aiming to illuminate its capabilities and challenges. It proposes to scrutinize the effectiveness of DL in improving the diagnosis of complex cardiac conditions, thereby contributing to the advancement of personalized medicine and patient care.

The **second chapter** focuses on applying DL for predicting Fractional Flow Reserve (FFR) using Optical Coherence Tomography (OCT) and angiographic images. This chapter describes the steps involved in developing and validating DL models tailored for this purpose. Starting with data collection and preprocessing, it moves on to detail the training process of these models, highlighting how they're designed to accurately interpret OCT and angiographic images to predict FFR values. The core aim here is to improve the diagnosis and treatment planning for patients with cardiac diseases by offering a non-invasive method to assess coronary artery conditions. Through a methodical approach, this chapter presents the outcomes of applying DL models in medical imaging, discussing both their effectiveness and the challenges encountered during the process. The work contributes to the ongoing efforts in enhancing cardiac diagnostics, aiming to provide a reliable tool that can support clinical

decisions without the need for invasive procedures.

The **third chapter** explores the challenge of detecting collateral circulation within coronary angiographies through the lens of DL. The section begins by detailing the compilation of the dataset used for training and validation, emphasizing the critical role of high-quality, clinically relevant data in the development of effective DL models. It then transitions into a technical exposition of the process involved in designing, training, and refining DL models specifically engineered to identify signs of collateral circulation from angiographic images. The chapter meticulously examines the validation of these models against the diagnoses of clinical experts, providing a rigorous assessment of their accuracy and reliability. Through this analytical journey, the chapter aims to highlight the potential of DL to augment the current methodologies used in diagnosing coronary artery diseases, particularly in complex cases where traditional imaging techniques may fall short. Furthermore, this chapter discusses the implications of successful collateral circulation detection for patient treatment plans and outcomes, underscoring the significance of this advancement in cardiac care. By tackling the challenges and showcasing the successes in applying DL to this aspect of cardiac diagnostics, the chapter contributes valuable insights into the potential of machine learning technologies to improve medical imaging and, consequently, patient care.

The **fourth chapter** delves into the realm of DL for the intricate task of aortic valve detection, state classification, and aortic stenosis assessment using echocardiography images. The chapter commences by outlining the process of gathering and preparing echocardiography data, setting the stage for the development of DL models specifically designed for the nuanced detection and classification of aortic valve conditions. The narrative then progresses to detail the innovative methodologies employed in creating these DL models. It explains the selection of model architectures that are most suited to capture the subtle features indicative of various aortic valve states and the severity of aortic stenosis. Emphasis is placed on the iterative process of model training, fine-tuning, and validation, highlighting the critical role of accuracy and reliability in the diagnostic capability of these models. By presenting a comprehensive exploration of the challenges and breakthroughs in applying DL to aortic valve diagnostics, this chapter contributes significantly to the broader narrative of enhancing cardiac care through advanced imaging technologies. The insights shared here aim to pave the way for further innovations in the field, ultimately improving patient outcomes in the management of valvular heart diseases.

The **fifth chapter** investigates the application of DL in automating the detection of myocarditis using Cardiac Magnetic Resonance Imaging (CMRI) scans. It begins by discussing the data collection process, emphasizing the significance of diverse and clinically representative CMRI views to train the DL models effectively. The chapter then details the methodology behind developing DL models capable of distinguishing myocarditis from CMRI scans, exploring the preprocessing techniques used to enhance image quality and the selection of model architectures optimized for this task. The narrative further delves into the model training process, elucidating the strategies employed to maximize the models' diagnostic accuracy. Special attention is given to the selection of the most informative CMRI views for myocarditis detection and the exploration of features critical for the models' decision-making processes during inference. This section assesses the reliability and accuracy of the DL models in diagnosing myocarditis, highlighting their potential to augment current diagnostic methodologies by providing rapid and non-invasive detection capabilities. By showcasing the challenges, successes, and implications of this research, it contributes valuable perspectives on the integration of DL into cardiac diagnostics.

The **final chapter** synthesizes the findings and insights garnered from the application of DL across various cardiac diagnostic challenges addressed in the preceding chapters. This final chapter offers a reflective overview of the research journey, summarizing the key contributions of the thesis to the field of medical imaging and cardiac diagnostics. It emphasizes how DL models have been meticulously developed and validated to improve the diagnosis of cardiac diseases, from predicting FFR and detecting collateral circulation to identifying aortic valve issues and diagnosing myocarditis using advanced imaging techniques. Looking forward, the chapter outlines the avenues for future research,

acknowledging the limitations encountered in the current study and suggesting strategies to overcome them. It proposes areas where further investigation could yield significant advancements, such as improving model interpretability, exploring the application of DL in other cardiac conditions, and integrating these technologies into clinical practice.

2. Towards a Deep-Learning Approach for Prediction of Fractional Flow Reserve from Optical Coherence Tomography and X-ray Angiography[1]

Introduction
FFR from OCT
FFR from OCT and X-ray Angiography
Discussion and Conclussions

2.1 Introduction

Cardiovascular disease (CVD) is the number one cause of death worldwide, and coronary artery disease (CAD) is the most prevalent CVD, accounting for 42% of these deaths. In CAD patients, plaque builds up in the coronary arteries and limits the blood flow to the myocardium, especially when the demand is increased (exercise, stress). In severe cases, this can lead to myocardial infarction, or even death.

X-ray coronary angiography (XA) represents the gold standard in CAD imaging [94]. Optical coherence tomography (OCT) is used in certain scenarios in conjunction with XA. OCT has the highest resolution among all invasive imaging modalities, allowing for a precise intra-vascular evaluation of stent apposition and expansion [95, 96, 97] thus, representing a paramount tool for PCI (percutaneous coronary intervention) optimization [98]. Nonetheless, its ability to assess the functional significance of a stenosis is not negligible [99].

The purely anatomical assessment of CAD, independent from the medical imaging modality, does not fully capture the functional significance of coronary stenoses. In view of the limitations of the anatomical evaluation of CAD, Fractional Flow Reserve (FFR) has been introduced as a functional index. FFR is defined as the ratio of flow in the stenosed branch at hyperemia—a condition of stress, with maximum coronary blood flow—to the hypothetical hyperemic flow in the same branch under healthy conditions. This can be shown to be closely approximated by the ratio of hyperemic cycle-averaged pressure distal to the stenosis to the cycle-averaged aortic pressure [100]. An FFR value ≤ 0.8 is considered to be positive, i.e., the patient requires invasive treatment, such as percutaneous coronary intervention (PCI-stenting) or coronary artery bypass graft (CABG). An FFR value > 0.8 is considered to be negative, i.e., typically only optimal medical therapy is prescribed. Several clinical

[1] The following section contains work published in:

- **Hatfaludi, Cosmin-Andrei**, et al. "Towards a deep-learning approach for prediction of fractional flow reserve from optical coherence tomography." Applied Sciences 12.14 (2022): 6964. https://doi.org/10.3390/app12146964
- **Hatfaludi, Cosmin-Andrei**, et al. "Co-registered optical coherence tomography and X-ray angiography for the prediction of fractional flow reserve." The International Journal of Cardiovascular Imaging (2024): 1-11. https://doi.org/10.1007/s10554-024-03069-z

The text were quoted verbatim from the above references, which represents previously published work of the author, under the PhD research program.

trials have demonstrated the superiority of FFR-guided decision-making [101], which represents the current gold standard. However, although providing obvious advantages, studies indicate that the use of FFR is still relatively low due to the need to administer hyperemia-inducing drugs, additional costs, and the extended duration and invasive nature of the procedure [102]. Hence, computational approaches for FFR prediction have been introduced, relying either on computational fluid dynamics (CFD) or on artificial intelligence (AI).

Blood-flow computations, performed using CFD, when used in conjunction with patient-specific anatomical models that are extracted from medical images, have been proposed for diagnosis, risk stratification, and surgical planning[97]. Model-based assessment of coronary stenoses has been previously performed using such techniques in several clinical studies, based on anatomical models that are reconstructed from coronary computed tomography angiography (CCTA) [103, 104, 105, 106], XA [107, 108, 109, 110, 111], or OCT [112, 113, 114, 115]. Computed FFR has been the main quantity of interest in these studies, all of which showed that computed FFR has good diagnostic accuracy compared to invasively measured FFR. The CFD models consist of partial differential equations, which can be only numerically solved, leading to a large number of algebraic equations. Due to the time-consuming process that is employed for reconstructing the anatomical model, and the computationally intensive aspect of the CFD models [116, 117], they are not used for intra-operative assessment and planning, where near real-time performance is required.

Alternatively, artificial intelligence-based solutions may be employed that are capable of providing results in real-time. To develop such solutions, a large database is required for the training phase, containing pairs of input-output data. The input data are represented by the anatomical information, while the output are invasive FFR [118]. Once the training phase has been finalized, the online usage provides results instantaneously. Such supervised machine learning (ML) algorithms are routinely employed in medical imaging applications, e.g., organ segmentation [119]. Moreover, machine learning models can also be employed to reproduce the behavior of non-linear computational models [120],[121].

Recently, machine learning models for the prediction of FFR based on CCTA[122], XA [123], OCT [124], and intravascular ultrasound (IVUS) [125] have been introduced. All these approaches rely on the extraction of features describing the vascular geometry, specifically the arterial lumen, and, in some studies, also on patient features.

With the study herein, we aim to predict the invasively measured FFR, exploiting the measured radius of the coronary lumen using the data of both OCT and angiography. In contrast to prior machine learning methodologies applied to the prediction of FFR, our approach diverges by employing unprocessed, dimensionality-reduced anatomical data as input features, as opposed to manually engineered features. A second pivotal aspect of our investigation pertains to our targeted examination of intermediate coronary lesions, wherein the conventional visual assessment of CAD using XA fails to provide a definitive clinical verdict. Consequently, our dataset encompasses a substantial cohort of lesions characterized by FFR values that closely approximate the critical threshold of 0.8, thereby intensifying the complexity inherent to the prediction task.

Deep-learning (DL) is a class of machine learning algorithms that uses multiple layers to extract higher level features from the raw input [126]. The FFR prediction task can be formulated either as a regression problem (predict the exact value of FFR) or as a classification problem (predict the FFR class, e.g., binary classification: ≤0.8 or >0.8). There are several types of neural networks that are suitable for the FFR prediction, amongst others:

- fully connected neural network, commonly referred to as artificial neural networks (ANNs). Potential disadvantages of ANNs are the large number of trainable parameters, which leads to the requirement of large training datasets, and the difficulty in capturing the inherent properties in 1D/2D/3D data structures

- convolutional neural networks (CNNs). Compared to ANNs, CNNs can capture the inherent properties in 1D/2D/3D data structures, but still require relatively large training sets. Also,

fixed size input data are required if the network is not fully convolutional.

- recurrent neural networks (RNNs) [127]. RNNs have the advantage that a variable length input sequence can be processed, but they may be affected by vanishing and exploding gradient issues.

Few-shot learning (FSL) is a type of learning where the prediction is performed based on a limited number of samples[128]. In a study that was published by Yang et al., the models that were used for FSL were classified into four categories: multitask learning, embedding learning, learning with external memory, and generative modeling.

OCT images were previously used in a variety of DL-based applications: stent strut detection [129, 130], stent strut segmentation [131, 132, 133], coronary calcification segmentation [134, 135], atherosclerotic plaque characterization [136], and lumen segmentation [137]. Furthermore, DL-based approaches were employed also in studies addressing other types of optical signals [138, 139].

Herein, we evaluate the performance of ANNs, CNNs, and RNNs in both regression and classification formulations. Additionally, we also consider the use of FSL, focusing specifically on prototypical networks [140], a subcategory of the embedding learning models, considered the state of the art for classification tasks. Our method relies on both OCT and Angiographic images. In the clinical environment, the clinical expert takes the diagnosis and treatment decision after inspecting images of both modalities.

2.2 DL based Prediction of FFR from OCT

2.2.1 Materials and Methods

2.2.1.1 Data Set

This was a single-center, retrospective study that was carried out at the Clinical Emergency Hospital, Bucharest, Romania. The study complied with the Declaration of Helsinki for investigation in human beings. The study protocol was approved by the local ethics committee and each patient signed an informed consent form before the enrolment in the study.

Patients at least 18 years old, with stable angina, and an indication for diagnostic XA due to intermediate or high likelihood of obstructive coronary artery disease, were considered. Further inclusion criteria were: at least one lesion with 40% to 80% diameter stenosis by visual assessment, and invasive FFR measurement considered required by the operator for clinical decision-making. Patients were excluded if they were unable to provide informed consent, had significant arrhythmia (heart rate over 120 bpm), suspected acute coronary syndrome, atrial fibrillation, low systolic pressure (below 90 mmHg), contraindication to beta blockers, nitroglycerin or adenosine, a non-cardiac illness with a life expectancy of less than 2 years, pathological aortic valve, rest state angina, or myocardial infarct during the last 6 months. Additionally, aorto-ostial lesions were excluded from the study. A total of 80 patients were included in the study.

Coronary angiography (Siemens Artis Zee, Forchheim, Germany) was performed after iso-centering in posterior-anterior and lateral planes, via a transradial (preferred) or transfemoral approach. In all cases, a 6 French diagnostic catheter was used after intracoronary injection of glyceryl trinitrate according to routine practice in the hospital, with manual contrast injection and cine acquisition at a frame rate of 15 frames/second. OCT imaging was performed using a frequency-domain OCT systems (St. Jude Medical/Abbott, St. Paul, MN, USA). The fiber probe was pulled back at a constant speed and cross-sectional images were generated with a spacing of 0.2 mm. The acquisition of physiological data for FFR calculation was performed according to conventional practice [141] with a commercially available FFR measurement system (PressureWire Aeris; St. Jude Medical, Minneapolis, MN, USA). The 0.014 coronary wire with a pressure tip was advanced until the pressure sensor passed the orifice of the guiding catheter. Transcatheter aortic and intracoronary pressure tracings

were equalized. Subsequently, the guidewire was advanced into the respective coronary artery until the pressure sensor passed the index lesion. Hyperemia was induced by the administration of adenosine either intravenously at a constant rate of 140 g/kg/min, or as an intracoronary bolus (100 g for the right and 200 g for the left coronary artery); the pressure recording was started, and the FFR was determined. A total of 102 coronary lesions in 80 patients underwent FFR analysis. This invasively measured FFR represents the ground truth that is used during the training of the deep neural networks, as described in the following.

The OCT data were exported from the OCT workstation available onsite. All OCT slices are RGB images, and the exported data contains the automatically detected coronary lumen, which is overlaid on the image and depicted in green. The spacing between the slices is 0.2 mm, and the number of slices per acquisition is constant at 376. Figure 2.1 displays the data pre-processing workflow starting from the exported OCT images with automatically detected lumen contour. First, the contours are automatically extracted by processing the green channel as follows: a threshold representing 90% of the maximum intensity value is used to create a binary image, and all the contours are extracted [142]. We then retain the contour which surrounds the center of the image: if there are multiple such contours, we pick the one with the largest area. Next, we use an in-house developed application to collect manual input that is provided by the clinical expert:

- selection of the proximal start and distal end slice, which define the coronary artery region of interest. Slices representing the catheter are excluded, alongside other slices with sub-optimal image quality (e.g., blood artifacts);
- rejecting/correcting erroneous contours within the selected slice-range: the automatically detected contours may be incorrect on certain slices, typically in bifurcation regions and/or if the lumen has a profoundly non-circular shape (e.g., concave shape). Erroneous bifurcation contours are rejected, while erroneous contours in the stenosis region are corrected (required in less than 10% of the OCT acquisitions).

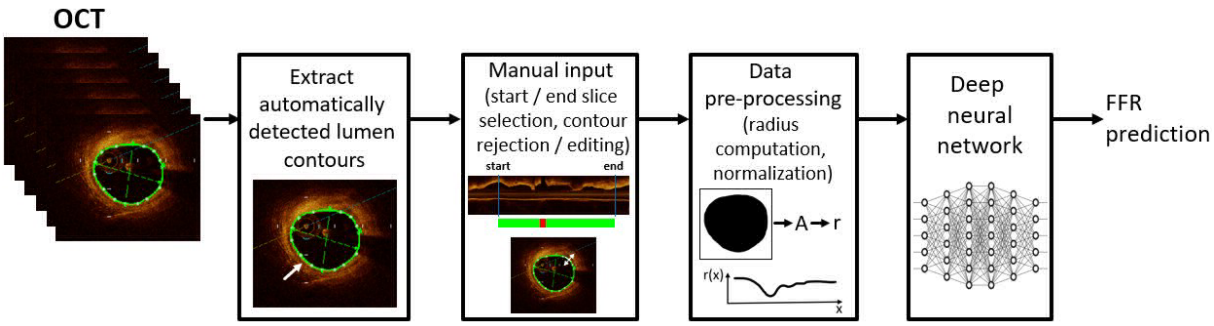

Figure 2.1: OCT data processing workflow, including FFR prediction using a deep neural network.

Next, the data are pre-processed: the inside area of each non-rejected lumen contour in the selected slice-range is computed and the effective radius is determined (considering an equivalent circular contour with identical area). The radius of rejected contours is set using linear interpolation that is applied on the radiuses of the closest neighboring contours that have not been rejected. The radiuses are then arranged in a 1D sequence, starting with the proximal slice of the selected slice-range. Since the OCT slices are equidistant, only the radius values are used as input. For the further processing using deep neural networks, the 1D radius sequence is padded to a size of 376 (maximum length of an OCT sequence), and z-score normalization is performed [143]. The mean and standard deviation of each acquisition are computed, and then a global mean and global standard deviation are computed for the training set by averaging the mean and standard deviation values of the acquisitions that are included in the training set. The acquisitions in the validation/test split are normalized using the values that are employed for the training set. The 1D sequence of normalized radius values is used as input for the deep neural network predicting FFR.

2.2.1.2 Deep Neural Network Based FFR Prediction

Different types of neural network models are considered for the prediction of the invasively measured FFR, ANNs, CNNs, and RNNs, applied with different approaches:

- a regression approach: models predict a rational number representing invasive FFR
- a classification approach: models predict the class of the FFR value (positive, i.e., FFR ≤ 0.8, or negative, i.e., FFR > 0.8)
- a FSL approach: similar to the classification approach.

As ANN, we used a fully connected neural network with 4 hidden layers, and the rectified linear unit (ReLU) [144] as the activation function for the hidden layers.

As CNN, we used a fully convolutional neural network (1D convolutions) with eight layers. For the hidden layers we used ReLU as activation function, and batch normalization was employed [145]. For the regression and the classification approach we added a final fully connected layer to perform the prediction. For the FSL approach, this layer is not required.

As RNN, we included a bidirectional gated recurrent unit (GRU) [146] layer on top of the previously described fully convolutional neural network (referred to as CNN + RNN in the appendix). This avoids the padding requirement. The CNN layers learn the relevant features from the input, and then the RNN performs the final prediction based on those features. Training a fully RNN network was not possible considering the small size of the available dataset. For the regression and the classification approach we added a fully connected layer after the bidirectional GRU to perform the prediction. For the bidirectional GRU, we used ReLU as the activation function.

No activation function was used on the last layer for the regression approach, and the sigmoid function [147] was chosen for the classification approach. For the FSL approach, the output of the network is represented by the features from the last hidden layer. The class is then determined by the smallest Euclidean distance between the output of the network and the two class clusters. These are defined by the mean features of the training set samples of each class.

For the classification and FSL approaches, all the samples with invasive FFR ≤ 0.8 represent the positive class and all the samples with invasive FFR > 0.8 represent the negative class. Since the dataset consists of only 102 invasive values, the models are evaluated using the leave-one-out cross validation strategy that is applied at the patient level [148]. For each fold, the samples of one patient are moved to a validation set, while the model is trained for a fixed number of epochs (300) on the samples of the remaining patients. The classification accuracy is computed for each epoch, and the epoch leading to the highest accuracy on the entire dataset, i.e., all folds, is chosen for reporting the statistics. Additionally, only during training of the classification-based approaches, we also ignored the samples with invasive FFR values in the range 0.79–0.81 (six samples). By removing these samples that are close to the cut-off point, the model is able to learn to better discriminate between the classes. For all the models we used the Adam optimizer [149], mean squared error as a loss function for the regression approach, and cross entropy [150] for the classification and the FSL approach (more details are included in Appendix A.2.). All the architectures were optimized using grid search [151], applied for: number of layers, number of neurons per layer, dropout percentage, and the learning rate. The implementation is based on Python, and the PyTorch [152] library for DL model training and inference.

To allow for a fair assessment of the performance, an ensemble approach is considered for each configuration: each of the proposed models is trained 20 times using different random seeds. For each configuration, the 20 models are then combined into one ensemble model. For regression approaches, the ensemble prediction for one sample is the mean value of the predictions of all 20 models. For classification and FSL approaches, the ensemble prediction for one sample is the mean value of the probabilities of all 20 models. This allows for a more robust assessment of the model performance, which is independent from the random seed that is used during training. The value 20 was

chosen following experiments which indicated that the ensemble model performance did not change when using larger values.

For all the ensemble models, we performed the receiver operating characteristic (ROC) analysis [153] and we computed the area under the curve (AUC) score [154]. Based on the ROC curves, we selected for each ensemble model the optimal cut-off point as being the point closest to the point (0, 1) [155]. The reported model performance metrics are based on the optimal cut-off point. The formula that is used to determine the point closest to (0, 1) is [156]:

$$ER(c) = \sqrt{(1 - \mathrm{Se}(c))^2 + (1 - \mathrm{Sp}(c))^2} \tag{2.1}$$

where ER is the closest point to (0, 1), c is a cut-point, Se is sensitivity, and Sp is specificity.

Similar to other studies, we further consider the minimum lumen diameter (MLD) and percentage diameter stenosis (%DS) as simple baseline references to assess the performance of the DL models. The %DS is computed as follow:

$$DS = (1 - -r_{\mathrm{min}}/r_{\mathrm{avg}}) \times 100 \tag{2.2}$$

Where r_{min} is the minimum radius of the sequence, r_{avg} is the average of the proximal and distal reference radius values of the lesion, as extracted from the OCT data.

For both MLD and %DS, we also apply the leave-one-out cross validation strategy at the patient level, as follows: for each fold, a threshold value is chosen which balances sensitivity and specificity on the respective training set, and then this threshold is applied to classify the test sample(s).

To evaluate the results, we computed the diagnostic statistics (accuracy, sensitivity, specificity, negative predictive value (NPV), and positive predictive value (PPV) [157] for all approaches, and additionally the mean absolute error (MAE), mean error (ME), and the mean squared error (MSE) for the regression approach. For the diagnostic statistics we additionally computed the 95% confidence intervals.

2.2.2 Results

2.2.2.1 Population Characteristics

Baseline patient and lesion characteristics are summarized in Table 2.1 and Table 2.2: 80 patients (66 male, 14 female) with 102 lesions were included in this study. The mean patient age was 60.5 ± 11.2 years. The mean FFR was 0.80 ± 0.08, and 48 of the lesions were hemodynamically significant according to the criterion FFR ≤ 0.80.

Table 2.1: Baseline patient characteristics and risk factors.

Male	66 (82%)
Female	14 (18%)
Age (years)	60.5 ± 11.2 years
Race	All Caucasian
Weight	81.93 ± 16.15 kg
Height	172.13± 8.05 cm
Diabetes	27 (33.75%)
Hypertension	60 (75%)
Hypercholesterolemia	62 (77.5%)
Smoking history	42 (52.5%)
Family history of CAD	3 (2.9%)
Previous myocardial infarction	46 (45%)
Previous Angina	64 (80%)
Ejection fraction	48.28 ± 6.31%

Table 2.2: Baseline lesion characteristics (n = 102).

Index Artery	
Left Anterior Descending artery (LAD)	57
Left Circumflex artery (LCx)	20
Right Coronary Artery (RCA)	25
Fractional Flow Reserve	
Mean ± SD	0.80 ± 0.08
Median (IQR)	0.83 (0.75-0.86)
FFR ≤ 0.80	48
FFR <0.75	25
0.75 ≤ FFR ≤ 0.85	47
FFR >0.85	30

2.2.2.2 Invasive FFR Prediction Performance

Figure 2.2 displays the ROC curve, the AUC scores including their 95% confidence intervals (CI), and the closest point to (0, 1) for all the approaches. The best three approaches based on AUC score are regression CNN, FSL RNN, and FSL CNN. Interestingly, the AUC score is superior for the regression CNN approach, but the FSL CNN approach has the closest point to (0, 1), i.e., the best diagnostic performance statistics, as shown below.

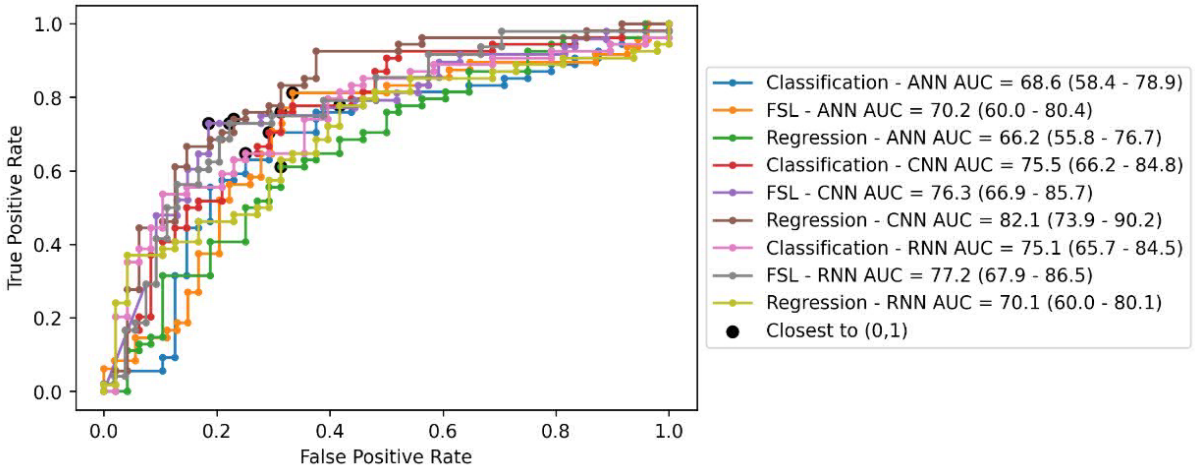

Figure 2.2: The ROC curve, AUC score, and the closest point to (0, 1) for all approaches. Values in the parentheses represent the 95% confidence intervals computed as in [158].

The performance and statistics of the various ensemble DL models and approaches considered herein are displayed in Table 2.3.

In terms of diagnostic performance, the FSL approach is performing better than classical regression and classification, while in terms of AUC, the CNN regression is superior to other methods. Since the 95% confidence intervals overlap, the differences are statistically not significant. FSL algorithms have been designed for optimal performance on small datasets where they tend to perform better than classic models. The best performing architecture is the one that is based on CNN. Furthermore, the training accuracy suggests that overfitting is not present for eight of the nine approaches. For the classic CNN-based classification, the model seems to overfit, even though different attempts were made to address this: L2 regularization and dropout. For comparison, MLD has an accuracy of 67.64%, a sensitivity of 64.81%, and a specificity of 70.83%. The %DS has an accuracy of 63.72%, a sensitivity of 62.96%, and a specificity of 64.58%. Each ensemble model consists of 20 models that were trained with different seed values. Table 2.4 displays the mean accuracy, the standard devi-

Table 2.3: Diagnostics and performance statistics of the considered ensemble DL models and approaches. Values in the parentheses represent the 95% confidence intervals.

Approach	Ensemble Arch.	Train Accuracy [%]	Accuracy [%]	Sensitivity [%]	Specificity [%]	NPV [%]	PPV [%]	AUC [%]	MAE	ME	MSE	Corr.
Regression	ANN	73.7	64.7 (55.1-73.3)	61.1 (47.8-80.1)	68.8 (54.7-80.1)	61.1 (47.8-73.0)	68.8 (54.7-80.1)	66.2 (55.8-76.7)	0.062	0.007	0.105	0.273
	CNN	85.9	75.5 (66.3-82.8)	74.1 (61.1-86.7)	77.1 (63.5-86.7)	72.5 (59.1-82.9)	78.4 (65.4-87.5)	82.1 (73.9-90.2)	0.082	-0.008	0.015	0.342
	RNN	69.7	68.6 (59.1-76.8)	77.8 (65.1-89.6)	58.3 (44.3-71.2)	70.0 (54.6-85.4)	67.7 (55.4-78.0)	70.1 (60.0-80.1)	0.072	0.022	0.011	0.261
Classification	ANN	78.4	70.6 (61.1-78.6)	70.4 (57.2-83.3)	70.8 (56.8-81.8)	68.0 (54.2-79.2)	73.1 (59.7-83.2)	68.6 (58.4-78.9)	-	-	-	-
	CNN	98.7	72.5 (63.2-80.3)	75.9 (63.1-88.7)	68.8 (54.7-82.1)	71.7 (57.5-85.9)	73.2 (60.4-86.0)	75.5 (66.2-84.8)	-	-	-	-
	RNN	73.8	69.6 (60.1-77.7)	64.8 (51.5-79.0)	75.0 (61.2-85.1)	65.5 (52.3-76.6)	74.5 (60.5-84.7)	75.1 (65.7-84.5)	-	-	-	-
FSL	ANN	78.9	72.5 (63.2-80.3)	79.2 (65.7-92.3)	66.7 (53.4-79.8)	78.3 (64.4-88.1)	67.9 (54.8-81.0)	70.2 (60.0-80.4)	-	-	-	-
	CNN	78.6	77.5 (68.4-84.5)	72.9 (59.0-86.8)	81.5 (69.2-89.6)	77.2 (64.8-89.0)	77.8 (63.7-91.5)	76.3 (66.9-85.7)	-	-	-	-
	RNN	75.6	75.5 (66.3-82.8)	72.9 (59.0-86.8)	77.8 (65.1-90.0)	76.4 (63.7-89.1)	74.5 (60.5-88.7)	77.2 (67.0-87.4)	-	-	-	-

ation (std) of the accuracy, the minimum accuracy (min), and the maximum accuracy (max) for the validation dataset when employing the default operating points/thresholds of 0.8 for regression and 0.5 for classification. While all variations are quite small, the smallest std is obtained for the models that are based on FSL, which further underlines the robustness of this approach. Additionally, we computed the ensemble model mean uncertainty by averaging the uncertainty of the ensemble model for each examination [159]. The ensemble model uncertainty for regression approaches is the standard deviation of the predictions of all models for one sample. An intuitive approximation for the ensemble model's uncertainty for classification and FSL approaches was chosen as: where y(i) is the ensemble model prediction for each sample and N is the number of samples; this uncertainty measure is the distance between the output probability and the predicted class label (0 or 1), therefore, predictions such as 0.1 or 0.9 are considered "confident" while others such as 0.4 or 0.6 are considered more "uncertain". This approximation is feasible since ensemble models usually have well-calibrated outputs [159]. The ensemble uncertainty results of the regression approaches are not directly comparable to the ensemble uncertainty results for the classification and FSL approaches, and it has been also shown [159] that regression-based uncertainty that is computed as the ensemble predictions' standard deviation is not well-calibrated as the MSE training loss "is not a scoring rule that captures predictive uncertainty" [159]. For the regression approaches, RNNs tend to have the smallest uncertainty. For classification and FSL approaches the uncertainty is similar for five of the approaches, while FSL CNN has a much smaller uncertainty.

The reason the default thresholds were employed in Table 2.4 is that selecting a best-operating-point with respect to some metrics and some held-out test-set is part of a post-processing stage; uncertainty estimates, however, depend solely on two factors: the input samples (i.e., input noise, out-of-distribution, etc.) and the learned model (here, the training procedure, the network architecture, and especially the training set have a large influence); the ground-truth label of a test input sample has no influence on the prediction uncertainty. Therefore, for an unbiased assessment, un-

Table 2.4: Diagnostic performance statistics of the considered ensemble DL models and approaches.

Accuracy						
Approach	Ensemble Arch.	Mean [%]	Std [%]	Min [%]	Max [%]	Uncertainty [%]
Regression	ANN	61.57	4.55	53.92	70.59	4.48
	CNN	61.76	2.65	55.88	65.69	12.91
	RNN	63.19	3.82	54.9	71.57	2.25
Classification	ANN	68.43	1.69	65.69	72.55	32.55
	CNN	67.75	3.1	63.73	73.53	32.9
	RNN	68.04	1.71	64.71	71.57	31.69
FSL	ANN	66.67	3.34	59.8	72.55	30.9
	CNN	75.59	1.2	72.55	76.47	2.77
	RNN	74.46	1.37	71.57	76.47	34.71

certainty measures of all the approaches were computed from the raw ensemble predictions and compared with the mean accuracy that was obtained from using the default thresholds.

2.3 Discussion and Conclusions

2.3.1 Deep Learning-Based Prediction of FFR

As more data are emerging from studies that are based on artificial intelligence and computational modelling, the incremental diagnostic value of predicted coronary functional diagnostic indices over the traditional XA-based visual or quantitative lesion grading is becoming more evident.

In this study, we have presented a novel approach for predicting Fractional Flow Reserve (FFR) through the application of deep learning, utilizing data from both optical coherence tomography (OCT) and angiography imaging modalities. It is noteworthy that we did not impose specific acquisition protocols for either OCT or angiography. Our investigations have demonstrated the promising potential of this method in the evaluation of functionally significant stenoses. We explored various models and methodologies, ultimately finding that the model, which combines OCT and angiographic data, exhibited superior performance. This is to be expected since the two imaging modalities are complementary. OCT has the highest image resolution, but the vessel length captured in the image is limited to 7.5cm. Furthermore, due to various artefacts (blood, etc.) typically only a shorter length fulfils image quality criteria. As a result, especially in case of multiple serial lesions, not all lesions are included in the OCT sequence that is input to the deep neural network, and there is a loss in FFR prediction accuracy. Angiographic on the other hand data has no limitation in terms of vessel length, but the image resolution is much lower. Hence, while all relevant lesions are included in the angiographic sequence that is input to the deep neural network, the accuracy of the radius information is sub-optimal. Additionally, angiographic images are 2D projections of the 3D vessel structure, which may further hide or distort certain anatomical details. It is important to also emphasize that the statistical analysis revealed no significant differences in the results obtained with the different input data settings (substantial overlap in their respective 95% confidence intervals). This is also given by the relatively small dataset size.

Thus, the main findings of this study can be summarized as follows: (1) DL-based FFR prediction from reduced-order raw anatomical data is feasible in a dataset that is focused on intermediate lesions for which the visual anatomical assessment of CAD based on XA does not allow for a clear clinical decision, and with no restriction on the type of lesions that were included in the study, and on the OCT acquisition; (2) DL-based FFR prediction provides superior diagnostic performance compared to baseline approaches based on MLD or %DS; (3) the FFR prediction performance increases

quasi-linearly with the dataset size, indicating that a larger training dataset will likely lead to superior diagnostic performance.

The diagnostic accuracy of 77.5% (OCT) and 84.3% (angio + OCT) achieved herein is lower compared to that of other studies focusing on FFR prediction from OCT, which reported an accuracy ranging between 88% and 95% [114, 115, 124, 160, 161]. There are two main aspects that are responsible for this difference. First, the complexity of the dataset that is processed herein is higher than that of other studies: 46% of the samples have an invasive FFR value ranging between 0.75 and 0.85, while in other studies these grey zone lesions represented between 20% and 44% of the entire dataset [114, 115, 124, 160, 161].

Secondly, past studies focusing on FFR prediction from OCT either rely on computational fluid dynamics (CFD) [114, 115, 160, 161], or on ML-based approaches including hand-crafted features [124]. By applying a deep neural network directly on the raw data that are represented by the effective radius along the centerline of the vessel of interest, we allow the model to automatically learn powerful features for FFR prediction. The results that were obtained in other application areas (healthcare or others) demonstrate that classic machine learning (ML) techniques and hand-crafted features typically outperform DL-based approaches when the training set is small, but, conversely, the DL-based approaches outperform classic ML-based approaches when the size of the trainset increases significantly [160]. The results in Figure 4, depicting the accuracy as a function of the dataset size, confirm that a larger dataset will enable a better performance: the performance of the DL model increases quasi-linearly with the dataset size. As shown in Table 3, the diagnostic performance of the proposed model is already considerably higher outside of the 0.75–0.85 FFR value interval.

To increase the prediction performance of DL models, different types of regularization are employed in the literature: mathematical expressions added to the loss function (L1, L2 regularization) [161], dropout (used to randomly drop out neurons during training) [162], and data augmentation [163]. Herein, we have used L2 regularizations and dropout. Data augmentation, i.e., generating new samples by perturbing the input data, is difficult to perform when training against invasively measured FFR, since the approximation of the ground truth values is not straightforward. We have considered data augmentation by adding a small amount of noise to the 1D radius sequence used as input, but the results have not improved.

A DL- or ML-based prediction of FFR was considered also in studies relying on other types of medical images (CCTA, XA). Kumamaru et al. [164] proposed a DL model to estimate invasive FFR from CCTA. They had a dataset containing 207 measurements from 131 patients and have obtained an accuracy of 75.9% in predicting an abnormal invasive FFR (≤0.8). Another interesting approach was proposed by Zreik et al. [165], they used DL in an unsupervised manner and obtained an overall accuracy of 78% on CCTA data. They obtained an accuracy of 66% for FFR < 0.7, 75% for an FFR between 0.7 and 0.8, 79% for an FFR between 0.8 and 0.9, and 73% for an FFR > 0.9. Itu et al. [122] proposed a DL model that was trained on ground truth values computed with a CFD-based approach on a database of synthetically-generated coronary anatomies. They achieved an accuracy of 83.2% on CCTA data.

3. Deep Learning Based Detection of Collateral Circulation in Coronary Angiographies[1]

Introduction
Data and CCC detection
Experimental results
Discussions and conclussions

3.1 Introduction

3.1.1 Introduction

Cardiovascular disease (CVD) is the leading cause of mortality and morbidity for the entire world population [54]. The most frequent cause of CVD is atherosclerosis [55], an inflammatory disease that gradually obstructs arteries and has life-threatening effects when present in the coronary circulation, i.e. leading to coronary artery disease (CAD). While traditional CAD risk factors (e.g., age, gender, diabetes, etc.) [56], as well as genetical risk factors [57] are highly predictive of the onset of CVD, mortality and morbidity is determined by clinical events such as the occurrence of ischemic tissue damage, which cannot be well predicted from traditional CAD risk factors [58, 59, 60].

One of the factors which helps to avoid ischemic tissue damage, is the development of coronary collateral circulation (CCC) [61]. CCC is characterized by natural bypasses (collateral arteries) which start to form as a result of progressive blood vessel lumen constriction and blood flow restrictions. Recent clinical studies have demonstrated that well-functioning CCC can independently predict lowered mortality and improved survival rates [62, 63]. The protective effect translates to improved left ventricular (LV) function, decreased remodelling, and a lower risk of life-threatening arrhythmias [64]. Thus, CCC can be regarded as a survival advantage [65].

Technical methods to automatically detect CCC currently lack behind studies on the clinical benefits of CCC. We aim to bridge this gap by introducing a novel method to detect the presence of CCC using deep neural networks on invasive coronary angiography (ICA) images. CCC detection represents an important prerequisite for assessing the morbidity rate for patients with CAD. Moreover, ICA is the gold standard in CAD. To the best of our knowledge, this is the first study to attempt CCC detection on ICA.

[1] The following section contains work published in:

- **Hatfaludi, Cosmin-Andrei**, et al. "Deep learning based detection of collateral circulation in coronary angiographies." 2023 IEEE 36th International Symposium on Computer-Based Medical Systems (CBMS). IEEE, 2023. `https://doi.org/10.1109/CBMS58004.2023.00337`

Some sections were quoted verbatim from the above reference, which represents previously published work of the author, under the PhD research program.

3.1.2 Background and Related Work

As mentioned earlier, no previous studies have attempted to detect CCC from ICA. Nevertheless, some studies focused on the assessment of CTO (chronic total occlusion) collaterals from ICA, detecting the onset of coronary artery disease, and on the evaluation of collaterals in patients with ischemic stroke using CT brain scans.

L. Liu et al. [66] proposed a deep learning based method for collateral physiology assessment under total occlusion conditions. Their model automatically extracts the length or time curves of the coronary filling to perform the assessment. H. Kuang et al. [67] proposed a vessel segmentation method for automating collateral scoring on brain CT angiography using a hybrid CNN transformer network. L. Wolff et al. [68] assessed a commercial algorithm for automated collateral scoring on brain CT angiography. Unfortunately, technical descriptions of the algorithm are not provided. Nevertheless, when tested against experts, the agreement between the algorithm and the experts is not significant.

M. Aktar et al. [69] proposed a deep learning method for collateral evaluation in patients with ischemic stroke using CT angiography. Their model processes 2D slices from CTA and uses a voting scheme to determine the outcomes. An additional difficulty of CCC detection is that, due to the myocardial contraction, the coronary vessels display a significant motion during a cardiac cycle.

Moreover, processing ICAs or CTAs with deep learning methods has a long background, for tasks such as coronary arteries segmentation [70], calcium scoring [71] or cardiovascular hemodynamic prediction on bypass surgeries [72].

Since the available data set for our task is small, a relevant related field is that of few-shot learning, with applications to deep learning. FSL is a learning method in which predictions are performed based on a limited number of samples [166]. Few shot learning (FSL) methods are classified into four categories: multitask learning, embedding learning, learning with external memory, and generative modeling. Herein we use prototypical networks [167], a subcategory of the embedding learning models, considered the state-of-the-art for classification tasks.

3.2 Data and CCC Detection

3.2.1 Dataset

For the CCC detection we operate in a low data regime, using a data set that consists of 239 patients (with 501 ICAs) for which CCC was annotated, and 285 patients (with 503 ICAs) without CCC. Some patients have multiple ICAs but for each patient we have at least one ICA. For the ICAs with CCC, only one frame was annotated, marking the location of the CCC.

To annotate the data, we developed a custom, Python-based, annotation tool that allows clinical experts to perform the annotation of ICAs with CCC. The tool enables experts to annotate the location of the collateral artery, the donor artery and the receiving artery, Rentrop grading [168], pathways [169], collateral flow grade [170], blush grade [171], the donor segment, the receiving segment, and the collateral artery size. We use these annotations for the subgroup analysis and for a future CCC quantification model. To reduce annotation time, the experts were asked to annotate only one frame for each angiography with CCC

The annotators were trained and supervised by expert interventional cardiologists with at least 10 years of experience in the catheter lab, and annotations were checked reciprocally and, in case of disagreement, discussed by at least two independent experts.

3.2.2 CCC Detection

To perform CCC detection while also balancing hardware resources, we extract from each angiography 11 consecutive frames. For the sequences annotated with CCC, we use five frames before the annotated frame, the annotated frame, and five frames after the annotated frame. While

more frames may be used, the computational costs increase significantly, and the information gains decrease since the contrast flushes out over time. For the sequences without CCC, we employ a model that is described in section III.C to compute the vesselness score and select 11 frames centered around the frame with the highest vesselness score. All data is normalized using z-score normalization [172] across the spatial pixel intensities.

To extract spatial features from the selected frames we use a spatial CNN (backbone) with six layers meant to capture a large field of view. The extracted spatial features are later concatenated and processed by 2D convolution with a kernel size of one, that extracts spatial and temporal features from the sequence. Based on the extracted characteristics, a FC layer outputs a binary decision for each frame (whether CCC is present or not). For this reason, a sigmoid function [173] has been applied at the output of the network. If the predicted value is greater than 0.5, the CCC is present, and if the predicted value is less than 0.5 the CCC is not present. The goal of this layer is to extract both spatial and temporal features from all frames. An illustration of our approach is depicted in Figure 3.1.

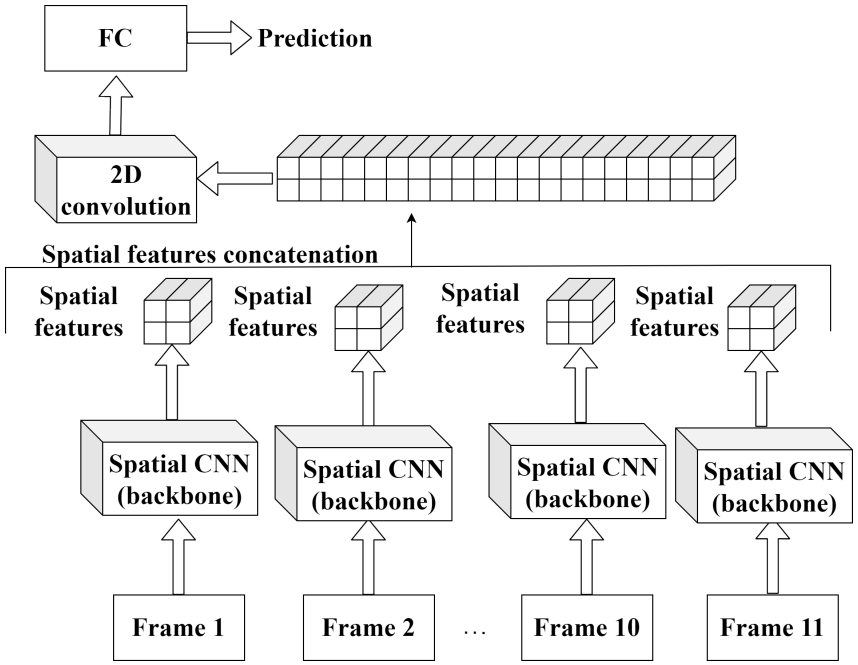

Figure 3.1: The proposed method for the CCC detection.

The spatial CNN is used in three configurations: no pretraining, pretrained without freezing the weights of the backbone, and pretrained with freezing the weights (and training just the last convolutional and fully connected layers). The pretrained backbone uses an auxiliary task of segmenting the vessels.

The models are trained using a vanilla method and a method based on prototypical networks. Due to the low data regime we operate in, we trained the models using k-fold cross validation [174] with k = 4, for 100 epochs. The k-fold cross validation datasets are split at patient level, meaning that all ICAs from one patient belong to the same fold. The classification accuracy is computed for each epoch, and the epoch leading to the highest accuracy on the entire dataset (all folds) is chosen for reporting the statistics. All models are trained using Adam optimizer [175] and a fixed learning rate of 0.0001.

To analyse the features that the model is focusing on, the saliency maps were computed [176] for the models obtained on the views leading to the highest accuracy. To obtain the saliency map for those models, the derivative of the output with respect to the input for each individual model was computed.

3.2.3 Backbone Pretraining

To boost the performance of the vanilla model, we also pretrained the backbone on a proxy task and performed transfer learning on the CCC task. For pretraining, we used a supervised learning vessel segmentation task, for which annotations were already available. An illustration of the task is provided in Figure 3.2.

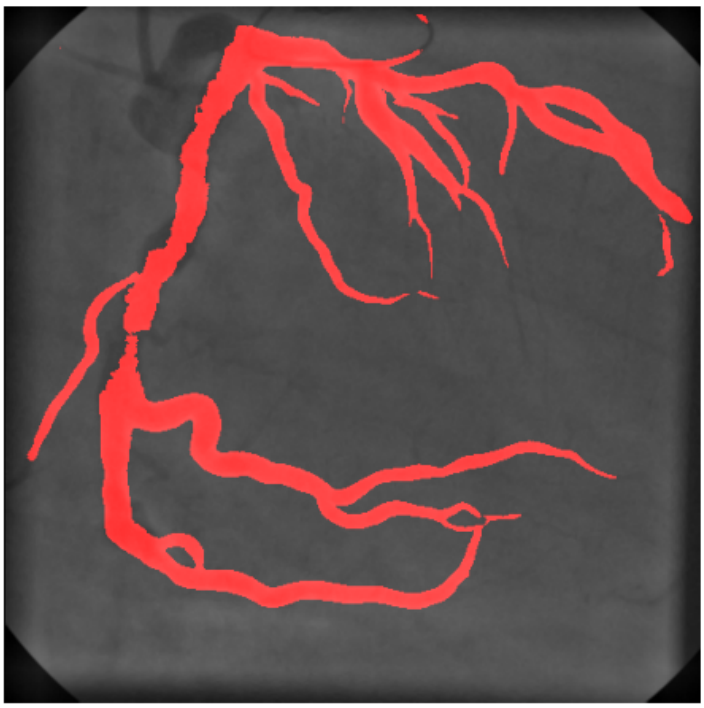

Figure 3.2: The predicted vesselness segmentation for a dicom from our dataset.

To generate ground truth masks, we had access to annotated artery centerlines and diameter information. From these, we generated segmentation masks using a Gaussian function (with mean centered on the centerline points and a standard deviation of 0.75). The Gaussian ensured smooth vessel edges. To preserve smoothness, we formulated the training process as a regression problem, and used MSE as loss (instead of thresholding the segmentation masks and employing classification loss functions). In total, we had access to 3350 ICAs for pretraining, from which we used 70% for training, 10% for validation and 20% for testing. Training ran for 100 epochs and we used early stopping based on the minimum loss on the validation data set. The evaluation on the test set revealed a Dice score of 0.92 (with sensitivity 0.95 and specificity 0.94).

3.3 Experimental Results

3.3.1 CCC Detection

To evaluate the CCC detection performance, we determined the accuracy (Acc.), sensitivity (Sens.) and specificity (Spe.) [177]. The results obtained on the entire dataset following cross-validation, using all models described in previous section, are illustrated in Table [**fig:tablecols1**]. The table indicates that the best results are obtained using a FSL model with pretraining and with weight freeze. All models perform better if the backbone is pretrained. Fig. 5 displays four sample cases from the dataset: one true positive (TP), one true negative (TN), one false positive (FP), and one false negative (FN). We observe that both the FP and the FN samples are difficult, as the FP image has artifacts which can easily be confused with CCC and the FN sample's field of view looks incomplete.

Table 3.1: Results obtained for the CCC detection.

Model	Pretrain	Freeze	Acc. [%]	Sens. [%]	Spec. [%]
Classic	✗	✗	55.2	55.6	54.8
	✓	✗	76.9	78.4	75.3
	✓	✓	77.2	82.2	72.3
FSL	✗	✗	57.8	58.2	57.4
	✓	✗	79.1	80.2	78.1
	✓	✓	80.0	79.0	81.1

To further analyse our best-performing model for CCC detection, we explored the model's decision-making process using saliency maps, a technique that visually represents which features significantly influence the model's predictions. By calculating the gradient of the model's output relative to its input, we generated these maps to pinpoint the critical areas within angiographic images the model deems important. Figure 3.3, showcasing the saliency map, reveals that the model predominantly bases its predictions on the detection of vessels. This finding is significant as it aligns the model's focus with the critical elements of CCC detection, emphasizing the importance of vascular structures in the diagnostic process. The saliency map not only confirms that the model is learning relevant patterns but also offers insights into improving model accuracy and interpretability by highlighting the specific features it examines.

Additionally, this approach enhances the model's transparency, a vital factor in medical diagnostics, by illustrating its reliance on clinically relevant features. The use of saliency maps, therefore, not only validates the model's effectiveness but also supports its potential integration into clinical settings by demonstrating its focus on meaningful diagnostic indicators.

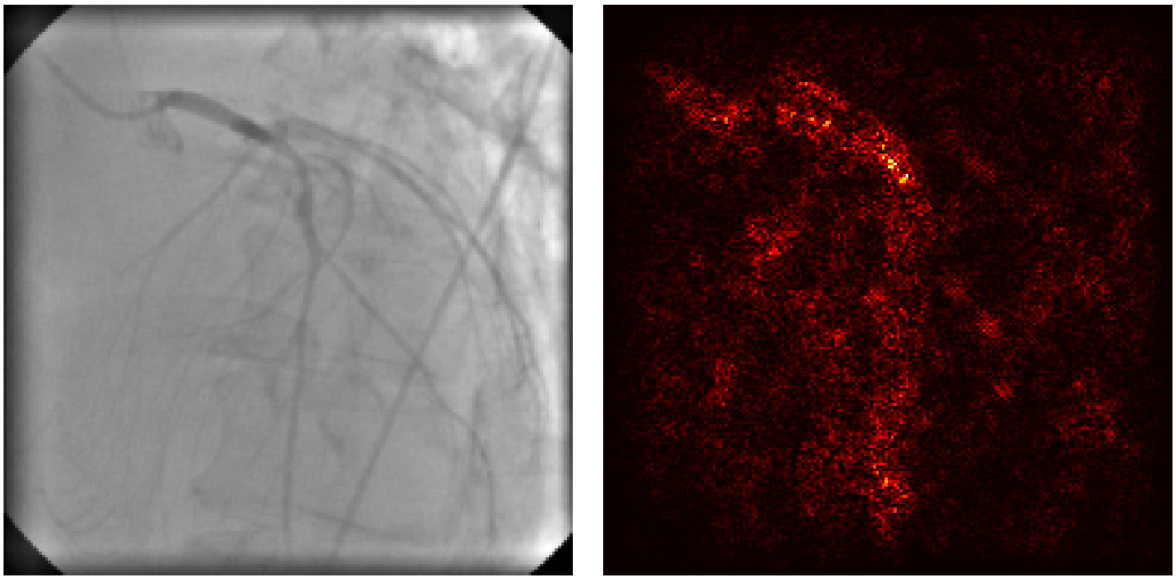

Figure 3.3: The saliency map of an image for the best performing model.

3.4 Discussions and Conclusions

Overall, the models introduced show promising results for CCC detection, albeit the performance can be further improved. One of the main challenges was the small dataset size. We approached this

problem from two angles: (i) by pretraining the models, and (ii) by employing few shot deep learning techniques. However, the lack of data and population diversity induces small inconsistencies in the results, which we discuss in this section.

As shown in Table 3.1, pretraining provided significant improvements for both classical and few shot learning. This motivates further research into better pretraining methods, using more data. For our task, we had annotated data and formulated pretraining and a supervision task. However, if more data without annotations are available, self-supervised methods deserve exploration [178].

The use of few shot learning techniques further provided marginal improvements. However, as shown in Table3.1, these improvements were not entirely consistent. For example, when using the pretrained backbone without freezing the weights, classical training exceeded few shot learning. This result is likely because optimizing the prototypes and fine-tuning the backbone weights was not possible given limited training data set. When freezing the weights, however, the prototypes could be better defined and the few shot method exceeded classical training. This balance between choosing which parameters to specialize in limited data regimes deserves future exploration.

3.4.1 Conclusions

In this study, we introduced a pioneering deep learning-based methodology for detecting CCC ICAs images, navigating the challenges posed by low data regimes. Leveraging a CNN-based architecture, our method adeptly integrates both spatial and temporal features, harnessing the power of pretraining on coronary segmentation and employing few-shot learning techniques to overcome the limitations of sparse data availability.

Our comprehensive approach, underscored by multiple subgroup analyses, not only elucidates the nuanced outcomes of CCC detection but also sets a precedent for methodological rigor in the field. The integration of expert annotations played a pivotal role, facilitating a robust evaluation framework that compared our machine learning model's performance against a consensus among experts.

This comparison revealed that, despite the ensemble model's slightly lower accuracy, its superior sensitivity makes it an invaluable asset in clinical settings, particularly where the cost of missing a condition is significant. The ensemble model's distinct sensitivity profile, coupled with the insights garnered from expert comparisons, underscores the potential of machine learning to augment traditional diagnostic processes, especially in the realm of CCC detection. This synergy between computational models and human expertise paves the way for enhanced diagnostic accuracy, promising to redefine the standards of patient care in cardiovascular diagnostics.

For future research, our focus will shift towards amassing a more diversified dataset and extending the model's capabilities through self-supervision and landmark-based CCC detection. By doing so, we aim not only to refine the core task of CCC detection but also to explore CCC quantification, thereby broadening the horizons of our research and its applicability in clinical practice.

In conclusion, our study marks a significant step forward in the application of deep learning for cardiovascular diagnostics. By innovatively combining spatial and temporal data analysis with the strategic use of limited datasets, we have laid the groundwork for future advancements in the field. As we continue to evolve our model and expand our dataset, we remain committed to improving CCC detection, with the ultimate goal of enhancing patient outcomes through the power of artificial intelligence and machine learning.

4. Deep Learning Based Aortic Valve Detection and Aortic Stenosis Detection on Echocardiographies[1]

Introduction
Materials and methods
Experimental Results
Conclussions

4.1 Introduction

Aortic stenosis (AS) is the most common heart valve injury encountered in clinical practice, and affects 2% to 5% of older adults. These estimates, together with an expanding elderly population, have significant implications for both resource allocation and public health. Echocardiography is the main non-invasive imaging method for assessing the aortic valve (AV), aortic stenosis and decision-making [75]. The etiology of aortic stenosis is largely explained by degenerative processes [76]. There is no medical therapy available to delay or correct these processes, and standard treatment is based on AV replacement. The current recommendations for AV replacement in patients with AS are based solely on the presence of: (i) severe AS based on a scoring system that includes specific valve criteria, and (ii) the presence or absence of symptoms related to AS. The prognostic significance of a comprehensive classification of staging of cardiac lesions in patients with AS has recently been demonstrated [77]. In the case of certain subclasses, e.g. low flow, patients with low gradient AS, asymptomatic patients, the recommendations are inaccurate and there are no recommendations on the importance of the various anatomical and functional cardiac consequences of AS. Patients with low gradient AS represent 35-40% of patients with moderate or severe aortic stenosis [78]. Misinterpretation of these patients can lead to either an inappropriate delay in AV replacement and increased mortality, or to an unnecessary valve procedure. Incorporating echocardiographic and clinical data into an AI (artificial intelligence) model to determine the severity of AS would potentially help in distinguishing these subgroups of patients, optimize the treatment decision, and improve long-term outcome. The thorough assessment of AS is based on a large number of measurements extracted from echocardiographic images in B and Doppler mode, leading to lengthy echocardiographic examinations [79]. Multiple studies have demonstrated the ability to successfully perform automatic echocardiographic recognition and interpretation of common 2D and 3D structures and parameters and disease states using artificial intelligence (AI) and, in particular, deep learning (DL) [80, 81, 82, 83]. A very recent study attempted to identify severe AS from echocardiography using DL [84]. To date, there is no automated or AI-based approach to conducting a comprehensive assessment of AS in echocardiography.

[1] The following section contains work published in:

- **Hatfaludi, Cosmin-Andrei**, et al. "Deep learning based aortic valve detection and state classification on echocardiographies." 2022 IEEE 20th International Power Electronics and Motion Control Conference (PEMC). IEEE, 2022. 10.1109/PEMC51159.2022.9962953

Some sections were quoted verbatim from the above reference, which represents previously published work of the author, under the PhD research program.

The overarching objective of this research activity is to advance the assessment of aortic stenosis (AS) by developing an artificial intelligence (AI)-based model that not only detects the aortic valve (AV) and classifies its state (open or closed) using deep neural networks in parasternal long axis (PLAX) echocardiographic images, but also extends to performing a detailed staging classification to characterize the degree of cardiac impairment in AS patients. This activity sets out to enhance the current methodologies for diagnosing and stratifying AS risk, aiming to improve upon the limitations of existing clinical guidelines. The proposed model is designed to integrate and leverage advanced AI techniques for a comprehensive anatomical and functional evaluation of the aortic valve and heart, utilizing patient echocardiographic data. By combining the initial steps of detecting the AV and its operational state with a nuanced AI-based staging classification, this study seeks to provide a holistic approach to AS assessment, offering significant improvements in the accuracy and efficacy of diagnosing and managing aortic stenosis.

Deep Learning (DL) represents a subset of Machine Learning (ML) characterized by its use of multiple layers to progressively extract higher-level features from raw input data, offering a robust framework for tackling complex pattern recognition tasks [179]. The transformative impact of Convolutional Neural Networks (CNNs) on the field was not fully realized until 2012, when a groundbreaking system developed by Krizhevsky et al. clinched victory at the ImageNet competition, setting a new benchmark for image classification accuracy [180]. This victory marked a watershed moment, heralding the widespread adoption and development of CNNs in various domains of artificial intelligence. In the ensuing years, the literature has burgeoned with diverse CNN architectures, each designed to address specific challenges or improve upon the efficiency and accuracy of neural network training. Notable among these are the VGG network, which introduced the concept of using very small convolutional filters to deepen the network architecture [181]; ResNet, which implemented residual connections to facilitate the training of substantially deeper networks by mitigating the vanishing gradient problem [182]; and Darknet, known for its efficiency and utilization in real-time object detection systems [183]. Each of these architectures embodies a unique approach to harnessing the power of deep learning, contributing to the field's rapid evolution and its expanding capacity to solve increasingly complex computational problems. The continuous innovation in CNN architectures underscores the dynamic nature of deep learning research. As these models become more sophisticated, their applications extend beyond mere image recognition, impacting areas such as natural language processing, medical diagnosis, autonomous vehicles, and more. This evolution reflects not only the versatility of CNNs but also their potential to drive significant advancements across a broad spectrum of technological and scientific fields.

The Faster R-CNN algorithm represents a significant advancement in the realm of object detection within images, distinguished primarily by its superior processing speed [184]. This algorithm stands out among its predecessors, including R-CNN [185], Fast R-CNN, and SPP-Net, by dramatically reducing the time required for image analysis. Specifically, the Faster R-CNN completes image processing in approximately 0.2 seconds, a stark contrast to the 2.3 seconds required by Fast R-CNN, the 4.3 seconds by SPP-Net, and the considerably longer 49 seconds by the original R-CNN. This leap in efficiency can be attributed to Faster R-CNN's innovative integration of a Region Proposal Network (RPN), which directly generates region proposals within the network, effectively streamlining the detection workflow. By embedding this step into the deep learning model itself, Faster R-CNN eliminates the need for the external region proposal algorithms that its predecessors relied on, thus significantly accelerating the object detection process. The enhanced speed and efficiency of the Faster R-CNN not only improve the practicality of deploying such models in real-time applications but also mark a pivotal development in the field of computer vision, paving the way for more sophisticated and timely object detection solutions.

Few-shot learning (FSL) refers to a machine learning approach where predictions are made using a small dataset [128]. According to research conducted by Yang et al., models designed for FSL can be categorized into four distinct groups: multitask learning, which involves training on multiple related tasks simultaneously; embedding learning, which focuses on creating representations that

encapsulate the essence of the data; learning that utilizes external memory, enabling the model to reference past information; and generative modeling, which generates new data samples based on the limited samples available.

4.2 Materials and Methods

4.2.1 Dataset

The dataset consists of 1886 PLAX echocardiographies. First, each echocardiography was re-sampled to a constant rate of 20 frames per second, and the first 20 frames were extracted, thus covering exactly one second of acquisition. Using predefined tags from within the Dicom header, a rectangular RoI was constructed around the ultrasound cone, while every pixel outside this region was set as background. Two scanlines were constructed starting from the reference pixel location of the acquisition, i.e., the top point of the cone and cutting into the ultrasound cone region. Their cutting angles were automatically tuned to obtain a tight fit around the cone sides. The initial cone RoI was further shrunk by these scanlines to remove any text annotations residing besides the original ultrasound cone. Next, two frames were selected and annotated, one where the valve is open and one where the valve is closed. A target-bounding box was placed around the AV, and the state of the valve was noted (open / closed).

On a subset of 699 echocardiographies, the medical experts annotated the presence of severe AS. The annotations are binary, 660 dicoms are annotated with the absence of severe AS and 39 are annotated with the presence of severe AS. We can observe that the dataset used for the detection of aortic stenosis is highly imbalanced.

The aim of the methods described below is to detect the AV, to classify the AV state for all the frames of an echocardiography and to detect the presence of severe AS.

4.2.2 Aortic Valve Detection

For the AV detection, we rely on the Faster R-CNN algorithm. The Faster R-CNN consists of a region proposal network (RPN) added on top of the Fast R-CNN network. First, the image is fed into the backbone. The output of the backbone is called features map. The RPN has the role of proposing regions for every point in the output feature map. To accomplish that, a set of anchors are placed on the input image for each location corresponding to a point in the features map. Next, the RPN has to check whether the anchors contain an object, and to refine these anchor coordinates to provide bounding boxes. The anchors that contain an object are called regions of interest (RoIs). All anchors that contain an object are than pooled to the same dimension (256x7x7) using a region of interest pooling layer (ROI pooling). This type of layer was proposed for the Fast R-CNN, and it has the role of extracting equal-length feature vectors for all proposals, i.e., RoIs, from the features map.

Finally, the output of the RoI pooling layer is passed to a fully connected layer that has the role to predict the class scores (softmax layer) and to predict the final bounding boxes (regression) of the detected objects.

The block diagram for this approach is depicted in Figure 4.1.

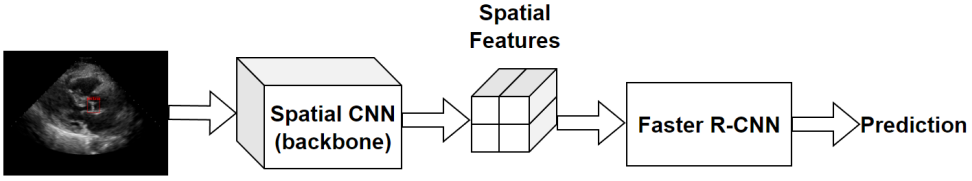

Figure 4.1: The proposed approach for the AV detection.

A two-dimensional CNN is first used to extract the spatial features from the image frame. Based

on the extracted spatial characteristics, the Faster R-CNN algorithm detects the AV, classifies its state (closed / open), and extracts the characteristics of the AV. Although the focus at this stage lies on the localization of the AV, we also perform the AV state classification to force the model to learn features that are representative for the AV state, which is the target of the temporal model described in the next section. For training, we used the Adam optimizer [186] and the multi-task loss function described in [184]:

$$L(p_i, t_i) = \frac{1}{N_{\text{cls}}} \sum_i \left[L_{\text{cls}}(p_i, p_i^*) + \lambda \frac{1}{N_{\text{reg}}} p_i^* R(t_i - t_i^*) \right] \tag{4.1}$$

Where the classification loss L_{cls} is a log loss over the two AV state classes, R is the robust loss function (smooth L1), p_i is the predicted probability of an anchor noted with i being an object, p_i^* is the ground truth label, t_i represent the four parameterized coordinates of the bounding box, and t_i^* represent the ground truth coordinates.

For the AV detection, we used the entire dataset (1886 echocardiographies, i.e., 3772 image frames), which was randomly split it into three datasets as follows: 70%, 15%, 15% for training, validation and testing, respectively. The data is normalized using z-score normalization [187] across the spatial pixel intensities. We tested various architectures of VGG (VGG-16, VGG-19) and Resnet (Resnest-18, Resnet-50) as backbone.

4.2.3 Aortic Stenosis Assesment

In this section, the proposed approach for detecting AS in cardiac echocardiography is described. Utilizing the algorithms and applications discussed in previous subsections, a multi-task model incorporating attention mechanisms was proposed. The aortic stenosis detection application is based on the same aortic valve features extracted by the spatial CNN and detected using the Faster R-CNN algorithm. The method used to identify aortic stenosis is similar to the one applied for analyzing the cardiac cycle. In addition to the temporal CNN used for cardiac cycle detection, another temporal CNN was added to predict the presence or absence of severe aortic stenosis. The output of this model is binary, if the predicted output is greater than 0.5 presence of severe AS is detected and if the output is smaller than 0.5, no severe aortic stenosis was detected. To better understand the multi-task approach utilized in this subsection, Figure 4.2 includes the general concept of the multi-task approach. The B-mode echocardiography is processed by the spatial CNN and the spatial features are extracted for each frame. Based on the extracted features, the Faster-R CNN detects the aortic valve then extracts the aortic valve features that are passed to the cardiac cycle detection algorithm. This features alongside the cardiac cycle detection are passed to the AS assessment block, which then detects the presence of absence of the AS.

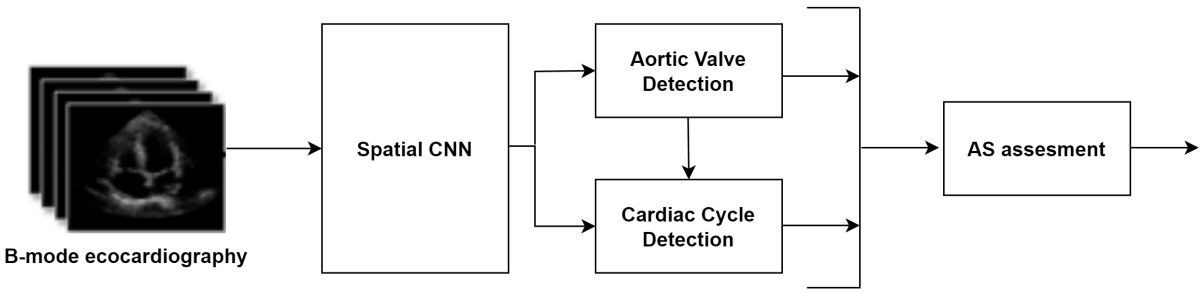

Figure 4.2: The multi-task approach used to detect the presence of severe AS.

For the AS assessment, we used only the annotated 699 echocardiographies. In this study, due to the constraints of a limited dataset, k-fold cross-validation [188] was implemented with k = 2 during

a training span of 300 epochs. Dataset partitioning for the cross-validation was executed, ensuring the initial distribution of the dataset class imbalance. For each training epoch, the weighted accuracy metric was computed, and the epoch that demonstrated the highest weighted accuracy across the entire dataset was selected for reporting the statistics. The models were consistently trained using the Adam optimizer with a learning rate maintained at 0.0001. The AS assessment model was trained using both classical approach and FSL.

Currently, the application of the Faster R-CNN algorithm has so far been limited to isolating features of the aortic valve through the use of a spatial convolutional network. Moving forward, we plan to extend the algorithm's functionality by applying it to identify areas significantly exceeding the typical dimensions of the aortic valve zone. To achieve this, we expand the AV predicted bounding box by a factor of 1, 1.5, 2, 2.5, and 3 in each direction. This adjustment is based on the hypothesis that an increased region of interest (ROI) could potentially enhance the precision in detecting severe aortic stenosis.

To ensure the robust validation of our Few-Shot Learning (FSL) model, we adopt a strategy that involves selecting random samples from the validation dataset to create both a support set and a query set. The support set serves as the basis for generating predictions for the query set. This dynamic selection process, where the support and query sets are constantly varied, implies that the volume of validation steps can significantly influence the observed accuracy. To accurately assess the model's performance, we devised an experimental approach where the model undergoes repeated validation phases until the accuracy levels off and stabilizes. This method is designed to mitigate variability in the validation process and provide a more reliable measure of the model's true predictive power. By continuously adjusting the composition of the support and query sets and observing the impact on accuracy over successive validation iterations, we can more precisely determine the model's efficacy in handling new, unseen data. This meticulous validation technique not only enhances our understanding of the model's capabilities but also ensures that the model is thoroughly tested across a wide range of scenarios, thereby bolstering confidence in its generalizability and real-world applicability.

4.3 Experimental Results

4.3.1 Aortic Valve Detection

The precision and recall metrics were used to evaluate the AV detection performance [189]:

$$\text{Precision} = \frac{TP}{TP + FP}, \tag{4.2}$$

$$\text{Recall} = \frac{TP}{TP + FN}. \tag{4.3}$$

We use IoU (Intersection over Union) as a metric to determine whether the AV was localized correctly [190]. Any detection with an IoU > 0.5 is considered a true positive detection (TP), any detection with an IoU ≤ 0.5 is considered a false positive detection (FP) and any image for which the network did not predict at least one object is considered a false negative (FN) detection. In addition, MIoU (mean IoU) was also calculated to assess how well the AV is detected on the entire data set. The results on the test set are displayed in Table 4.1.

The best results on the test set were obtained using a Resnet-50 backbone for the Faster R-CNN algorithm. The model achieves a precision of over 93% and a recall close to 100%. Although each of these architectures has shown promise in various domains of image recognition and object detection, the Resnet-50 backbone emerged as the most effective for our purposes, particularly in terms of balancing computational efficiency with high precision and recall rates. The Resnet-50 architecture's success can be attributed to its deep residual learning framework, which alleviates the vanishing gradient problem, thereby enabling the training of significantly deeper networks without

Table 4.1: Results obtained for the AV detection.

Backbone	Dataset	Precision	Recall	MIoU
VGG-16	Validation	92.11	99.33	0.73
VGG-16	Test	89.42	98.87	0.73
VGG-19	Validation	90.57	99.33	0.72
VGG-19	Test	85.22	99.77	0.71
Resnet-18	Validation	93.27	100	0.72
Resnet-18	Test	89.42	99.77	0.71
Resnet-50	Validation	96.23	99.33	0.75
Resnet-50	Test	93.27	99.77	0.74

a corresponding degradation in performance. This characteristic is particularly advantageous for the complex task of AV detection, where subtle features and variations need to be discerned accurately.

4.3.2 Aortic Stenosis Assesment

To evaluate the aortic stenosis assessment we computed the accuracy and the weighted accuracy. The results obtained for this approach are depicted in Table 4.2. We can observe that the best results are obtained using the FSL approach. This is expected since the FSL algorithm is specialized for small datasets with high imbalance of data. Using the FSL approach, our AS assessment model obtained an accuracy of 95.7% and a weighted accuracy of 90.3%.

Table 4.2: The results obtained for the AS assessment model.

Method	Dataset	Accuracy	Weighted accuracy	Mean weighted accuracy
Classic	Set 1	95.8	83.4	89.3
Classic	Set 2	95.7	95.2	
FSL	Set 1	94.2	87.8	90.3
FSL	Set 2	95.7	92.9	

In Figure 4.3, we present two illustrative cases for the evaluation of AS, showcasing the model's capability to accurately assess AS presence. The depicted images feature two AV's, one with AS and one without, highlighting the model's ability to differentiate based on anatomical discrepancies. Notably, the valve afflicted with aortic stenosis is visibly larger due to the pathological changes associated with AS, while the other valve appears smaller and within normal size parameters. This visual comparison underscores the model's precision in identifying and assessing the severity of AS by analyzing structural variations in the AV, further validating its effectiveness in the accurate diagnosis of AS.

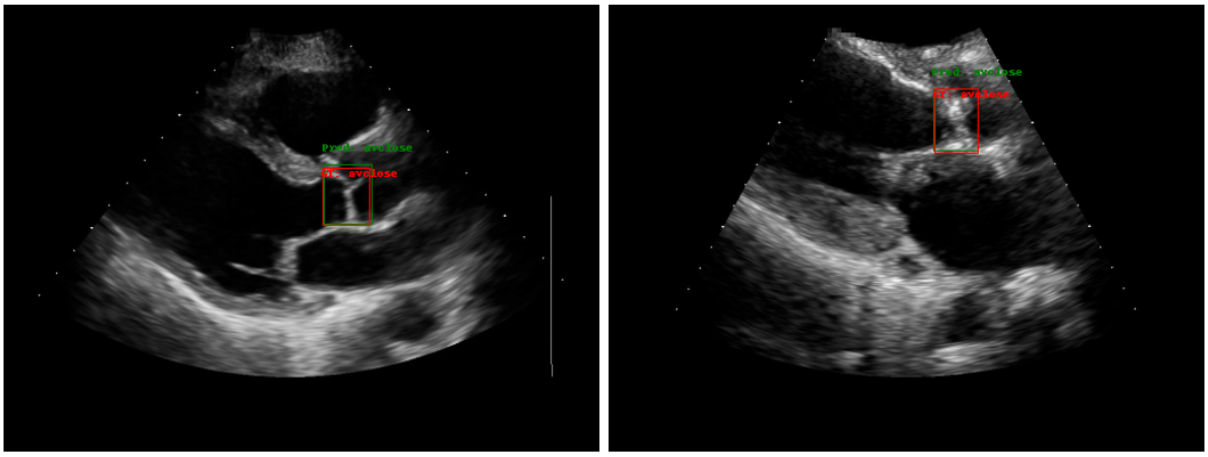

Figure 4.3: Sample predictions for AS assesment.

4.4 Conclusions

Within this research activity, a non-invasive method for detecting aortic stenosis using artificial intelligence has been proposed. Unlike current clinical guidelines, the proposed method eliminates the need for lengthy echocardiographic exams (both B-mode and Doppler), significantly reducing the time required to diagnose severe aortic stenosis in a patient. The algorithm offers a diagnosis based on 20 frames from a B-mode echocardiography, thereby removing the necessity for Doppler echocardiography. The proposed method achieves a detection accuracy of 96% for the aortic valve, 95% for the valve's state, and 91% for severe aortic stenosis. Aortic valve detection utilized the Faster R-CNN algorithm, enhanced with a post-processing module to correct misdetected dicom-level detections. To determine the state of the aortic valve (open/closed), a temporal convolutional network was employed, which makes a binary decision based on the features of the aortic valve. The outputs of these two models then serve as inputs for the automatic detection algorithm for severe aortic stenosis, deciding based on the aortic valve features and the cardiac cycle whether a patient has severe aortic stenosis. The parameters of the networks used, their hyperparameters, and other optimizations were empirically determined within this research activity. Two training approaches were utilized for the model: traditional training and training using a prototypical network. Prototypical networks require less training data, which impacts the cost associated with processing, collecting, and storing clinical patient data. Currently, no medical therapy for aortic stenosis can improve outcomes compared to the natural progression of the pathology, and there is no comprehensive, integrated diagnostic method for AS, nor any treatment decisions aimed directly at reducing risk and improving long-term outcomes. Severe aortic stenosis affects up to 5% of the global population, and with the aging population, it has a significant impact on public health. Therefore, there's a need for a more efficient and quicker solution for detecting severe AS, as well as a treatment scheme aimed at reducing long-term risk. This activity achieved the detection of severe aortic stenosis using cardiac ultrasound and AI, impacting the number of clinical tests needed to decide whether a patient has severe AS. Ultimately, requiring fewer clinical tests impacts the cost of diagnosing a patient with severe AS. AI could also be used to extract other clinical measurements from cardiac ultrasound. To improve the accuracy of the severe AS detection model, methods for extracting various relevant clinical measurements for aortic stenosis detection (e.g., automatic measurement of the LVOT diameter) will be investigated and later incorporated into the final severe AS detection algorithm.

Lai, Khin Wee, et al. [191] proposed a deep learning method based on image segmentation using AlexNet to detect the AV. They achieved an accuracy of 95% on 120 echocardiographies. Bin Ahmad

Nizar, Muhammad Hanif, et al. [192] proposed a deep learning method based on Faster R-CNN to detect the AV in echocardiography. They achieved a precision of 94.2% and a recall of 95.7%. In their study they only detected the AV with a bounding box but did not classify the AV state. They used 23 echocardiographies for training, five for validation and two for testing. J. M. Kwon et al. [193] proposed a deep learning algorithm based on CNN to detect aortic stenosis in electrocardiography that achieved an accuracy of 62%.

A precise detection of the AV and of its state are important prerequisites for the AS assessment. Future activities will focus on extending the proposed methods and integrating them into an AS assessment framework. The proposed DL based model can also be used as feature extractor or for pre-training an AV stenosis assessment model.

5. Automated Detection of Myocarditis from Cardiac Magnetic Resonance Imaging using Deep Learning[1]

Introduction
Materials and methods
Results
Discussions and conclussions
Limitations

5.1 Introduction

Myocarditis, characterized by inflammation of the cardiac muscle, has implications on both the myocardial contractile function and the electrophysiological properties of the heart, potentially leading to heart failure and arrhythmias, respectively [86]. This condition's etiology is multifaceted, encompassing infectious agents (for instance, viral pathogens like COVID-19 and parvovirus) [87], systemic inflammatory and autoimmune disorders, as well as adverse drug reactions. Clinical manifestations of myocarditis commonly include thoracic pain, lethargy, and dyspnea [88]. It is imperative for individuals presenting with symptoms suggestive of myocarditis to obtain prompt cardiological consultation to facilitate early detection and management. In cases of severe myocarditis, endomyocardial biopsy, a diagnostic intervention, is advocated to substantiate the diagnosis and inform therapeutic strategies [89]. Management of myocarditis includes a range of supportive measures, therapeutic interventions for symptomatic heart failure, administration of antimicrobial agents against identified infectious pathogens, and the use of immunosuppressive therapy in cases of severe inflammatory responses. Timely diagnosis and the immediate commencement of treatment are crucial in significantly reducing the associated morbidity and mortality. Non-invasive cardiac imaging, particularly cardiovascular magnetic resonance imaging (MRI) [194], plays a vital role in confirming the diagnosis of myocarditis. In their study on myocarditis, the authors [90]] underline the necessity of utilizing the Lake Louise Criteria (LLC) in cardiac MRI, which involves analyzing cine, T2-weighted black blood, and late gadolinium enhancement (LGE) images to accurately diagnose the condition. However, the interpretation of MRI is heavily reliant on expert analysis, which is both labor-intensive and susceptible to operator bias. To mitigate these challenges, the development of automated diagnostic systems utilizing advanced machine learning and data mining algorithms has been proposed. These systems are designed to efficiently address medical image classification challenges, thereby enhancing diagnostic accuracy and reducing subjectivity [91]. These technologies can be utilized

[1] The following section contains work published in:

- **Hatfaludi, Cosmin-Andrei**, et al. "Automated Myocarditis Detection Using Deep Learning and MRI." The International Journal of Cardiovascular Imaging - Under Review

The text were quoted verbatim from the above references, which represents previously published work of the author, under the PhD research program.

within reporting workflows to automatically screen images, which helps in saving time for physicians, minimizing the incidence of errors, and improving the accuracy of diagnoses.

Deep learning (DL) represents a category of machine learning algorithms characterized by the utilization of multiple layers to extract more abstract and advanced features from the raw input data [195]. Few-shot learning (FSL) is a learning approach in which predictions are generated using a limited quantity of samples [92]. According to Yang et al., the FSL models can be divided into four specific categories: learning with external memory, multitask learning, generative modelling, and embedding learning.

In the field of myocardial disease (MCD) diagnosis from cardiovascular magnetic resonance imaging (CMRI), recent years have seen significant advancements through the use of deep learning (DL) techniques, as evidenced by various studies [88, 93, 196]]. Sharifrazi et al. [88] introduced the CNN-KCL model, specifically designed for MCD detection using CMRI images, with testing conducted on the Z-Alizadeh dataset. This model incorporates a comprehensive approach by analyzing CINE-segmented images in both long axis (LAX) and short axis (SAX) views, Pre-contrast T2-weighted (TIRM) images in LAX and SAX views, T1-Weighted relative images pre-contrast and post-contrast in axial views of the myocardium, and Late Gadolinium Enhancements (LGE high-resolution PSIR) sequences in SAX and LAX views. The integration of these diverse views through a 2D-CNN with k-means clustering results in an impressive accuracy of 97.41%. Another noteworthy contribution by Shoeibi et al. [93] involved the application of the cycle-GAN method alongside various pre-trained models for MCD diagnosis, also utilizing the Z-Alizadeh dataset. The key innovation here was the use of cycle-GAN in preprocessing to generate synthetic CMRI images, which were then processed through different pre-trained models. Among these, the EfficientNet V2 method stood out, achieving an accuracy of 99.33%. Moravvej et al. [196] explored a different avenue by introducing deep reinforcement learning (RL) for MCD detection, presenting the RLMD-PA method for diagnosing myocarditis using CMRI images from the Z-Alizadeh dataset. Furthermore, the study examined various optimization methods to improve both the accuracy and efficiency of MCD diagnosis.

In this study, we introduce a deep learning (DL) approach designed to automate the detection of myocarditis from cardiovascular magnetic resonance imaging (CMRI). Our methodology evaluates multiple CMR image sequences to ascertain which produces the best separation between normal and myocarditis cases. Through a comparative analysis of different imaging views of the heart (short and long axis), we aim to identify the most effective imaging angle for myocarditis detection. This investigation is critical for refining diagnostic precision and could significantly impact clinical decision-making by providing insights into the optimal CMRI view for diagnosing myocarditis, thereby enhancing patient care and treatment outcomes.

5.2 Materials and Methods

5.2.1 Dataset

5.2.1.1 Study Design

This was a single-center, retrospective study that was carried out at the Center of Advanced Research in Multimodality Cardiac Imaging, Cardio-Med Medical Center, Târgu-Mureș, Romania. The study complied with the Declaration of Helsinki for investigation in human beings. The study protocol was approved by the local ethics committee and each patient signed an informed consent form before the enrolment in the study.

5.2.1.2 Study Population

Patients at least 18 years old, with atypical angina, dyspnoea and fatigue are indicated for performing a cardiac MRI. Further inclusion criteria were: history of cold/flu in the last 2-3 months,

changes on the electrocardiogram (sinus tachycardia, where T negative diffuse), fever and chills. Patients were excluded if they were unable to provide informed consent, and if they presented with myocardial ischemic injury (history of myocardial infarction STEMI and NON-STEMI), autoimmune diseases and infiltrative diseases at the myocardial level (amyloidosis). A total of 269 patients were included in the study, of whom 231 had myocarditis, while the remaining 38 were control subjects.

5.2.1.3 Procedure Protocol

Each patient included in the study was subjected to an MRI examination with consent. Based on the obtained results, patients were divided into the two study groups. To perform the cardiac scenarios, we used a doritonated MRI from Siemens, model Magnetom Aera, Forchheim, Germany.

A standard cardiac MR protocol was employed including cine balanced steady-state free precession (bSSFP) short and long axis views, T2-weighted acquisitions, and late gadolinium enhancement (LGE) in LAX 2-chamber and 4-chamber views. For the LGE acquisition a bolus of gadolinium-based contrast agent (Gadovist) was injected at a rate of 4 ml/s. Ten minutes after injection a phase sensitive inversion-recovery (PSIR) sequence was acquired at the same LAX positions as the cine bSSFP to detect LGE.

Following the suggestion of the clinical experts in the study, the following acquisitions were considered for the detection of myocarditis:

- PSIR LGE in 2-chamber and 4-chamber views (single frame)
- T2-weighted 2-chamber and 4-chamber views (single frame)
- Cine bSSFP in LAX 2-chamber, 3-chamber, and 4-chamber views (multi-frame)
- A SAX stack of cine bSSFP (x to y numbers) slices covering the left ventricle (multi-frame, multi-slice).

Figure 5.1. displays examples of all views. For the multi-frame views, we display the middle frame and for the multi-slice multi-frame view we depict the middle frame of the middle slice. We adapted a DL approach for each of the single frame, multi-frame, and multi-slice type of data to perform myocarditis vs. normal classification.

5.2.2 Data Preprocessing

All images were normalized using z-score normalization [197]. To potentially enhance the neural network's performance by focusing on the region of interest, the images were cropped. Given the central location of myocardium in the images, the cropping procedure was implemented as follows: we retained the central 50% of the image in each dimension plus a proportional segment (k) of the image size: $image_size/2 + k * image_size$. Parameter k was set at 0.5 (non-cropped images) and at increments of 0.05 ranging from 0.4 to 0.2. A separate DNN was then designed and trained for each view. Details are included in the following subsections.

To evaluate the performance we computed the weighted accuracy [198]:

$$\text{weighted accuracy} = 0.5 \times \frac{TP}{TP + FN} + 0.5 \times \frac{TN}{TN + FP}. \tag{5.1}$$

For the models that showed the highest weighted accuracy, receiver operating characteristic (ROC) analysis was performed as outlined in [199], and the area under the curve (AUC) score was calculated [200]. The selection of the optimal threshold for each model was guided by the ROC curves, identifying the point that most closely approached the ideal (0,1) coordinate, consistent with the methodology recommended in [201]. The chosen threshold was then applied to obtain the results, which are reported using various performance metrics (weighted accuracy, sensitivity, specificity, PPV, NPV) [202].

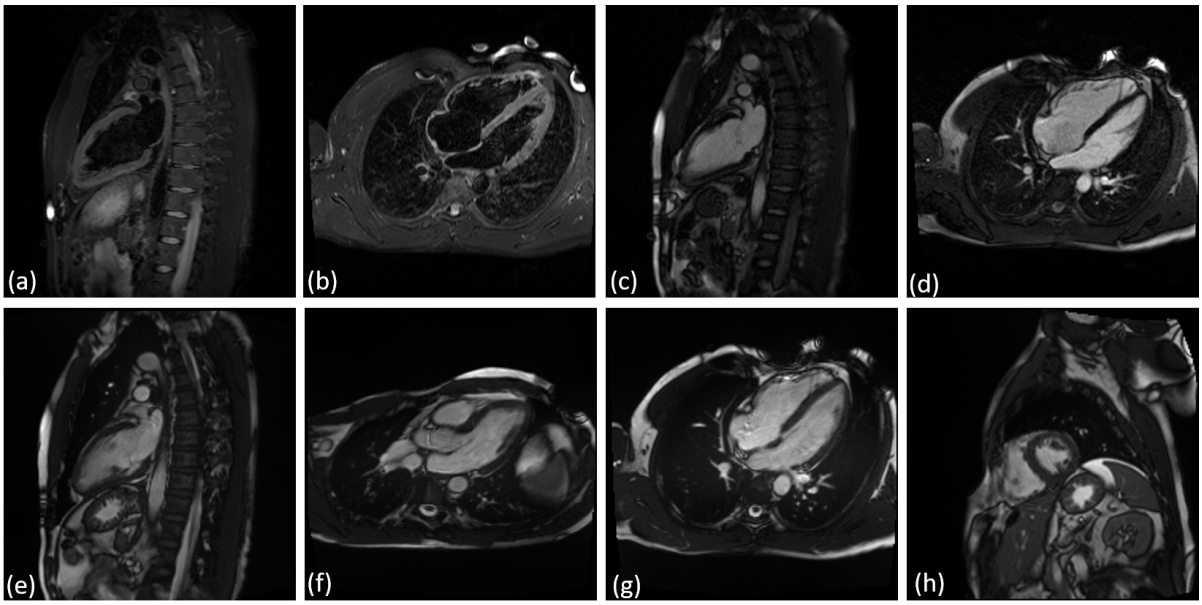

Figure 5.1: Views considered for the detection of myocarditis from cardiac MRI: (a) T2 weighted 2-chamber view, (b) T2 weighted 4-chamber view, (c) LGE 2-chamber view, (d) LGE 4-chamber view, (e) cine bSSFP 2-chamber view, (f) cine bSSFP 3-chamber view, (g) cine bSSFP 4-chamber view, (h) cine bSSFP SAX stack. The middle frame is displayed for multi frame views, and for the multi-slice multi-frame view, we used the middle slice and the middle frame.

The determination of the cut-off point closest to the coordinate (0,1) was achieved using the equation [203]:

$$\mathrm{E}R(c) = \sqrt{(1 - \mathrm{Se}(c))^2 + (1 - \mathrm{Sp}(c))^2} \tag{5.2}$$

Here, ER quantifies the shortest distance to the coordinate (0,1), c signifies the cut-off point, Se is sensitivity, and Sp represents specificity.

All the models were implemented using Python, specifically Pytorch. All statistical analysis were also performed in python.

5.2.3 Classification Based on Single Frame Images

The single-frame views were processed using a neural network architecture comprising six convolutional layers followed by a fully connected layer to generate the final output. The task was structured as a binary classification problem [204], and we adopted two distinct training strategies: a classical approach and a FSL approach. In the classic training paradigm, a sigmoid activation function [205] was utilized at the model's output layer to obtain probabilistic predictions ranging from 0 to 1. Conversely, for the FSL strategy, we omitted the terminal fully connected layer.

In this study, due to the constraints of a limited dataset, k-fold cross-validation [206] was implemented with k = 2 during a training span of 50 epochs. For the cross-validation process, the dataset was divided in such a way that all CMRIs from a single patient were grouped together into one-fold, guaranteeing that a patient's data would not be spread across multiple folds. Additionally, we ensured that a similar proportion of normal and myocarditis cases was present in the two splits. For each training epoch, the weighted accuracy metric was computed, and the epoch that demonstrated the highest weighted accuracy across the entire dataset was selected for reporting the statistics. The models were consistently trained using the Adam optimizer [207] with a learning rate maintained at 0.0001.

5.2.4 Classification Based on Multi Frame Images

For processing the multi-frame views, our approach involved using a spatial CNN (backbone) with six convolutional layers. The backbone was applied to individual frames independently. The resulting feature maps from each frame were then concatenated. Subsequently, a single 2D convolutional layer was applied to this aggregated feature set. The goal of this layer is to extract both spatial and temporal features from all frames. An illustration of our approach is depicted in Figure 5.2.

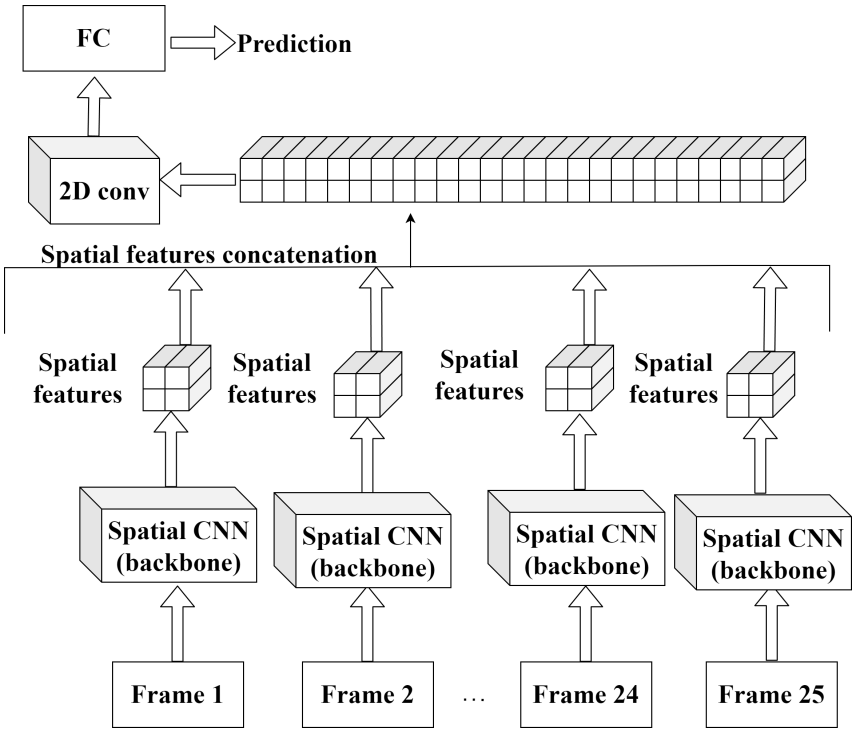

Figure 5.2: Illustration of the multi-frame processing approach using a spatial CNN backbone with six convolutional layers. This diagram depicts the process where the backbone is applied independently to each frame, followed by the concatenation of resulting feature maps from all frames. A subsequent single 2D convolutional layer is then utilized to extract and integrate both spatial and temporal features across the entire frame set.

Similar to the single-frame views, the task was defined as a binary classification problem. For this, we employed two distinct methodologies, consistent with the ones previously described for single-frame view analysis. All multi frame views have a fixed number of frames (25). For the stack of cine bSSFP SAX slices, each slice was processed independently using the approach depicted in Figure 5.2. The training of the model on this particular view was conducted under three different scenarios: first, by utilizing the complete set of slices for each patient; second, by employing a subset of three contiguous slices centred around the middle slice, and third, by selecting a broader subset of five slices centred around the middle slice (see Figure 5.3). For each scenario, we calculated the weighted accuracy to evaluate the model performance. Based on this outcome, the scenario with the highest accuracy was adopted for all subsequent experiments pertaining to this view.

5.3 Results

5.3.1 Population Characteristics

Baseline patient characteristics are summarized in Table 5.1.

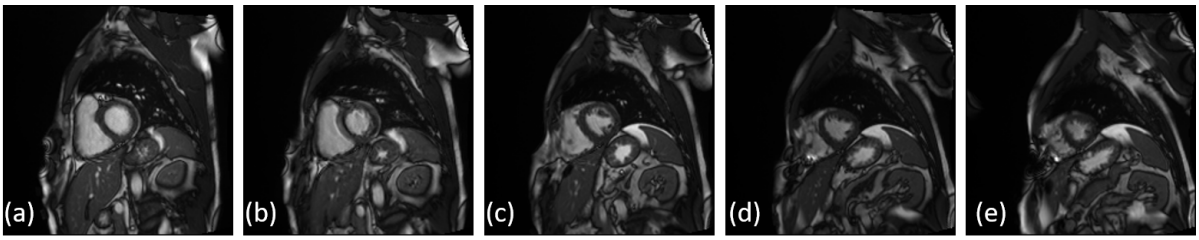

Figure 5.3: The five middle slices for the multi slice multi frame view (cine bSSFP SAX stack): a) slice 5, b) slice 6, c) slice 7, d) slice 8, e) slice 9. The middle frame is depicted for all 5 slices.

Table 5.1: Baseline patient characteristics and risk factors.

Male	137 (51.89%)
Female	127 (48.1%)
Age (years)	54.46 ± 15.87 years
Race	All Caucasian
Weight	75.01 ± 10.96 kg
Height	169.79 ± 7.13 cm
Diabetes	34 (12.84%)
HTA	193 (73.1%)
Hypercholesterolemia	156 (59.09%)
Smoking history	71 (26.89%)
Previous Angina	15 (5.68%)
FEVS	47.47 ± 4.58%

5.3.2 Cine bSSFP SAX Stack Results

The results obtained using the cine bSSFP SAX stack for classification are reported in Table 5.2. The best results for this view are obtained using three slices. This is to be expected since the myocardium is typically best visible in the middle slices. Hence, for all other experiments and results presented herein for this view, we have used a fixed number of slices equal to three.

5.3.3 All

The weighted accuracy computed for all the previously described models are reported in Table 5.3. The best results were obtained for PSIR LGE images in 2-chamber and 4-chamber views. On both views the model obtained an accuracy greater than 90%. On the single frame views the models achiever higher overall performance then on the multi frame views.

5.4 Discussions and Conclusions

In our study, we present a novel deep learning methodology for the detection of myocarditis from MRI scans. An optimal view for myocarditis detection was identified through rigorous evaluation. Comparative analyses demonstrated that the FSL approach outperformed the classical train-

Table 5.2: Weighted accuracy obtained for the cine bSSFP SAX stack, for different number of slices selected as input for the classification network.

View	Classic	FSL	Classic	FSL	Classic	FSL
Number of slices	All		3		5	
Weighted accuracy [%]	64.2	61.9	67.2	67.5	65.0	67.3

Table 5.3: Weighted accuracy obtained for the single- and multi-frame views considered in this study. In the table we reported the metrics for both Classic (Cls.) and FSL methods.

View	0.5 (original)		0.2		0.25		0.3		0.35		0.4	
	Cls.	FSL	Cls.	FSL	Cls.	FSL	Cls.	FSL	Cls.	FSL	Cls.	FSL
T2 weighted 2-chamber view	67.2	62.3	69.9	57.0	63.2	57.5	63.5	59.2	66.8	61.3	56.7	62.3
T2 weighted 4-chamber view	69.0	72.0	64.5	72.0	65.1	71.1	66.3	74.8	71.8	72.6	69.9	72.0
LGE 2-chamber view	93.0	96.9	86.6	87.2	84.4	88.1	85.7	87.0	91.4	90.7	89.2	95.6
LGE 4-chamber view	87.4	90.1	85.7	84.8	87.2	87.0	85.4	88.3	85.6	88.5	84.8	87.6
cine bSSFP 2-chamber view	66.3	67.3	75.0	75.8	67.9	76.8	70.7	73.5	66.1	75.2	68.2	72.9
cine bSSFP 3-chamber view	56.3	56.0	52.1	56.2	50.0	52.1	51.7	53.4	54.4	54.9	57.6	53.6
cine bSSFP 4-chamber view	56.3	63.0	56.7	61.7	63.0	63.1	59.2	62.6	64.4	60.2	62.6	64.3
cine bSSFP SAX stack (3 slices)	67.2	67.5	61.1	71.2	63.2	69.6	62.2	70.2	64.2	70.3	64.7	69.6

ing method across the majority of the views, underscoring its efficacy. Notably, the model exhibited robust learning capabilities even when trained on a small and highly unbalanced dataset, consisting of 231 cases with myocarditis against 39 without myocarditis. Feature analysis revealed that the model's predictions are predominantly based on characteristics derived from the myocardial region, indicating a targeted approach in identifying pathognomonic patterns indicative of myocarditis.

While all CMR image sequences considered for image-based classification: cine bSSFP, T2 weighted acquisitions, and LGE are clinically relevant and help guide the diagnosis according to [90], our DL classification method obtained the best results on the LGE images acquired in 2 and 4-chamber views. This suggests that the DL network can more reliably use features based on the presence of myocardial scar for the classification.

In the control group, which includes 39 cases, the artificial intelligence algorithm identifies 1 case as possibly positive for the diagnosis of myocarditis. The patient was in the 24-40 years range, and his history has identified a recent viral disease. However, the patient was clinically asymptomatic, and showed no changes in laboratory tests. MRI imaging of the patient showed a small punctate change in the myocardium, indicating possible microvascular damage at this level without clinical significance. This fact proves that the algorithm developed during this study has a high detection rate of changes, even minor, occurring at the myocardial level.

Analyzing patients in the myocarditis group, we found that the artificial intelligence algorithm identified from a total of 231 cases, 8 cases, as being false negative. These false-negative results were likely caused by diffuse distribution of a small amount of fibrosis in the myocardium, with patients presenting with forms of self-limiting myocarditis. A possible cause of these false negative results could also be the relatively small number of patients included in the group with myocarditis. Recent studies have proven that a larger number of patients included in the artificial analysis algorithm allows it to detect even those minor changes occurring in the myocardium.

In the area of myocardial disease diagnosis based on cardiovascular magnetic resonance imaging (CMRI), our study adopts an approach where each CMR image sequence is examined independently, a strategy that differs from those seen in prior studies like those by Sharifrazi et al.[88], Shoeibi et al. [93] and Moravvej et al. [196]. Our approach enabled a granular examination of how individual imaging views—ranging from T2-weighted acquisitions to LGE sequences—contribute distinctly to the accuracy and reliability of myocarditis detection. By evaluating the diagnostic performance of each view, our research not only identified the most effective sequences for myocarditis detection but also offered a rich, multi-faceted understanding of the disease's radiological presentation. This contrasts with the aggregated view analysis in other studies, which, while effective in harnessing composite information, may overlook the unique diagnostic value embedded within each specific imaging angle. The saliency analysis, in particular, offers valuable insights into what the algorithm considers important when making decisions, focusing more on how the model prioritizes different areas of the images for diagnosis. This saliency analysis, underscoring our model's reliance on features within the myocardial region, offers an interpretative depth not available in combined approaches, fostering a greater understanding of the patterns indicative of myocarditis. Through this strategy, our study contributes to the body of knowledge in cardiovascular magnetic resonance imaging.

6. Conclusions

Conclusions
Original Contributions
Dissemination of research results
Future Work

6.1 Conclusions

The thesis aimed to create, implement, and assess deep learning techniques on extensive datasets of medical imaging for cardiovascular disease diagnosis, with a specific focus on the nuanced diagnosis of vascular, valvular, and inflammatory cardiac diseases. The deep learning models were enhanced with tailored architectures, and the training processes were adapted to meet the unique requirements of each task, considering the diversity in data types, the complexity of predictions, and operational demands.

In the realm of medical imaging, integrating AI algorithms within imaging devices is becoming increasingly prevalent, enhancing diagnostic capabilities and streamlining routine tasks for efficiency in both time and resources. The effectiveness of these algorithms directly influences the practicality of diagnostic workflows. An essential aspect, alongside raw predictive power, is the capability to gauge prediction uncertainty. This not only elevates the transparency and reliability of automated medical evaluations but also enables the identification of cases with high uncertainty for expert review, thereby guiding subsequent actions or adjustments. To explore the aspects of uncertainty, the study focused on analyzing the uncertainty in FFR predictions and utilized saliency maps for the models discussed in the thesis. These maps revealed that AI holds significant potential in the medical sector, showcasing its ability to highlight critical areas and factors influencing model decisions, thereby reinforcing the viability and applicability of AI technologies in enhancing medical diagnostics and treatment planning. In addressing the challenge of limited annotation data, this study leveraged raw imaging data to pre-train DNNs using self-supervised heuristic pretext tasks, notably within CCTA imaging. This approach, although straightforward, required careful monitoring to avoid the influence of data artifacts that might align too closely with these tasks. Our exploration into DNN behaviors, particularly when introducing synthetic artifacts during training, highlighted a tendency of models to focus on exploiting these tasks rather than learning genuinely relevant features. To overcome the problem with the limited annotation data, the study also employed few-shot learning techniques, which are designed for effective training with minimal data, ensuring the extraction of meaningful insights from the available datasets.

In this thesis, deep learning (DL) models were utilized to diagnose vascular, valvular, and inflammatory cardiac diseases. For vascular diseases, DL models focused on CCC detection and FFR prediction, aiding in treatment decisions for coronary artery disease by identifying lesions requiring revascularization. Valvular disease diagnosis employed DL models for detecting aortic stenosis through echocardiography. Additionally, for inflammatory cardiac conditions, a DL model was developed for myocarditis detection, utilizing multiple views of CMRI.

6.1.1 Diagnosis of Vascular Cardiac Diseases using Deep Learning

This study marks a significant advancement in the use of deep learning for the diagnosis of vascular diseases, specifically through the applications of FFR prediction and CCC detection. By harnessing OCT and angiography, the research on FFR prediction demonstrated the ability of deep learning models to enhance diagnostic accuracy significantly over traditional approaches. The integration of these imaging modalities, each with its strengths and limitations, facilitated a more comprehensive assessment of coronary artery disease, particularly for lesions not clearly defined by visual examination. The exploration into regularization and data augmentation techniques, although with mixed outcomes, further emphasizes the potential for methodological enhancements to improve predictive performance.

Parallelly, the investigation into CCC detection using deep learning confronted the obstacle of small dataset sizes, employing strategies such as model pretraining and few-shot learning to mitigate this issue. Despite encountering inconsistencies, the effort to combine spatial and temporal data features through CNN-based architectures showed promising directions for future research. The necessity for a richer dataset and more refined methodologies was evident, with future work aimed at broadening data collection, applying self-supervised learning for pretraining, and optimizing few-shot learning techniques.

Collectively, these studies illustrate the transformative potential of deep learning in vascular disease diagnostics, suggesting a future where non-invasive, accurate, and efficient diagnostic methods are the norm. The success of these approaches could lead to a paradigm shift in how vascular diseases are diagnosed, offering improved pathways for treatment and patient care. As the field moves forward, the emphasis on expanding and diversifying datasets, alongside the refinement of deep learning models, will be crucial in overcoming current limitations and unlocking the full diagnostic capabilities of these technologies.

6.1.2 Diagnosis of Valvular Cardiac Diseases using Deep Learning

In this study, a complex deep learning framework was developed to precisely detect and classify the state of the aortic valve (AV) from echocardiography images, propelling forward the diagnostic capabilities for aortic stenosis (AS). By integrating the Faster R-CNN algorithm with an additional temporal CNN layer, the model goes beyond static image analysis to incorporate temporal information from sequential frames, ensuring a comprehensive assessment of the AV state over time. This method signifies a notable improvement over traditional detection techniques, which analyze each frame in isolation, by leveraging the temporal context to achieve a more accurate and dynamic understanding of the AV's condition. The approach has demonstrated remarkable success, reflecting in its superior precision and recall metrics when compared to existing methodologies. Such advancements underscore the potential of deep learning in revolutionizing the diagnosis of valvular diseases, offering a more efficient, non-invasive alternative that could significantly enhance patient outcomes and streamline clinical workflows.

6.1.3 Diagnosis of Inflammatory Cardiac Diseases using Deep Learning

A DL framework was introduced for diagnosing myocarditis using CMRI scans, significantly leveraging FSL techniques for enhanced detection accuracy. This approach was rigorously tested across various views to identify the most effective perspective for myocarditis identification, revealing FSL's superiority over conventional training methods in the vast majority of cases. The model demonstrated exceptional learning efficiency on a notably small and skewed dataset, comprising 231 myocarditis cases contrasted with 39 non-myocarditis cases. Through detailed feature analysis, it was discovered that the model primarily relies on specific myocardial characteristics to ascertain the presence of myocarditis, indicating its precision in detecting disease-specific patterns. Furthermore, the findings included the model's capability to identify subtle myocardial changes, suggestive of microvascular damage, even in clinically asymptomatic individuals. This high sensitivity to minor

myocardial alterations underscores the potential of advanced AI algorithms in revolutionizing myocarditis diagnostics, facilitating early detection and intervention. The occurrence of false negatives, attributed to the diffuse distribution of fibrosis or the dataset's limited size, points to the need for larger, more diverse datasets to refine the model's accuracy further. This research paves the way for more sophisticated, AI-driven diagnostic tools in cardiology, promising significant advancements in the early detection and treatment of myocarditis.

6.2 Original Contributions

The contributions made in this thesis are organized by the type of cardiac disease - vascular, valvular, and inflammatory. Each developed solution contributes towards the overarching aim in healthcare technology: to create reliable and credible systems for automating medical diagnostic processes, thereby enhancing the standard of patient care and service quality.

6.2.1 Diagnosis of Vascular Cardiac Diseases using Deep Learning

The integration of Optical Coherence Tomography (OCT) and angiography data as a combined input into Deep Neural Networks (DNNs) stands as a significant original contribution to the domain of FFR prediction. This novel strategy boosts the accuracy of FFR predictions, tackling the complexities of assessing functionally significant stenoses and harnessing the strengths of both imaging modalities to enhance diagnostic precision in coronary artery disease. Furthermore, **the use of an ensemble approach in conjunction with DNNs markedly improves FFR prediction, representing a significant advancement in non-invasive coronary artery disease diagnosis by integrating both imaging technologies for more accurate evaluations**.

A groundbreaking approach is introduced for the diagnosis of vascular cardiac diseases through deep learning, specifically focusing on the detection of CCC using invasive coronary angiography images. By creatively combining spatial CNNs for frame-based feature extraction with additional layers for temporal feature processing, the approach confronts the critical challenges of data scarcity through advanced pretraining and few-shot learning techniques. These contributions mark a significant leap in the application of artificial intelligence in cardiac care, setting the stage for more precise and efficient diagnostic tools in the management of vascular diseases.

6.2.2 Diagnosis of Valvular Cardiac Diseases using Deep Learning

The study introduces a sophisticated deep learning framework specifically designed for the detection and classification of the aortic valve (AV) state from echocardiography images, advancing the diagnostic capabilities for aortic stenosis (AS). This development represents a significant contribution by the authors, as it integrates the Faster R-CNN algorithm with an additional temporal CNN layer, enabling the model to incorporate temporal information from sequential frames for a comprehensive AV state assessment. This innovative approach signifies a notable improvement over traditional detection techniques by leveraging the temporal context to achieve a more accurate and dynamic understanding of the AV's condition, demonstrating superior precision and recall metrics compared to existing methodologies.

Another contribution of this research involves leveraging the aortic valve detection model as a foundational pretraining step for the aortic stenosis detection model. This technique, particularly through freezing the pretrained model's weights, enables effective learning on datasets where previously the significant class imbalance hindered learning capabilities.

6.2.3 Diagnosis of Inflammatory Cardiac Diseases using Deep Learning

The thesis delineates several pivotal contributions to the field of diagnosing inflammatory cardiac diseases using deep learning, with a focus on myocarditis detection using MRI scans. **The in-**

troduction of a novel deep learning methodology, crafted for automated myocarditis detection, incorporates both single-frame and multi-frame analyses, significantly advancing the accuracy of diagnoses derived from CMRI data. This methodology, conceived and developed within the study, achieved an impressive weighted accuracy of 96.9%, demonstrating the profound impact of deep learning models on improving myocarditis detection and potentially enhancing patient care through early diagnosis and treatment.

A notable contribution of this work is the effective application of Few-Shot Learning (FSL), which was found to outperform traditional training methods across most imaging views. This achievement addresses the prevalent challenge of analyzing small and highly unbalanced datasets in medical imaging, showcasing the researcher's adeptness at implementing cutting-edge solutions in complex diagnostic scenarios.

However, the research also candidly addresses challenges encountered, particularly with false-negative results attributed to the diffuse distribution of fibrosis in the myocardium. This transparency in acknowledging the limitations of the current models not only reinforces the integrity of the research but also paves the way for future improvements, marking a significant stride in the endeavor to refine deep learning applications in myocarditis detection and, more broadly, in cardiovascular disease diagnostics.

6.2.4 Summary of Contributions

Table 6.1: Summary of Contributions and Disseminations.

No. Order	Contribution	Subchapter	Dissemination article
1	The use of the ensemble model to enhance accuracy for FFR prediction. We used the prediction from 20 models combined into an ensemble for a better estimate of the FFR. Another advantage of using ensemble approach is that we can estimate the uncertainty for each prediction.	2.2.2	Hatfaludi, C. A., Tache, I. A., Ciușdel, C. F., Puiu, A., Stoian, D., Itu, L. M., ... & Scafa-Udriste, A. (2022). Towards a Deep-Learning Approach for Prediction of Fractional Flow Reserve from Optical Coherence Tomography. **Applied Sciences**, 12(14), 6964. DOI: 10.3390/app12146964
2	Another original contribution for the FFR prediction is using a combined approach that takes as input both the OCT signal and Angiographic signal. The mixed model accuracy increases significantly.	2.3	Hatfaludi, C. A., Tache, I. A., Ciusdel, C. F., Puiu, A., Stoian, D., Calmac, L., ... & Itu, L. M. (2024). Co-registered optical coherence tomography and X-ray angiography for the prediction of fractional flow reserve. **The International Journal of Cardiovascular Imaging**. DOI: 10.1007/s10554-024-03069-z

3	The original contribution here is based on a groundbreaking approach introduced for the diagnosis of vascular cardiac diseases through deep learning, specifically focusing on the detection of CCC using invasive coronary angiography images. By creatively combining spatial CNNs for frame-based feature extraction with additional layers for temporal feature processing, the approach confronts the critical challenges of data scarcity through advanced pretraining and few-shot learning techniques.	2.4.2	Hatfaludi, C. A., Bunescu, D., Ciuşdel, C. F., Serban, A., Böse, K., Oppel, M., ... & Itu, L. M. (2023, June). Deep learning based detection of collateral circulation in coronary angiographies. In **2023 IEEE 36th International Symposium on Computer-Based Medical Systems (CBMS)** (pp. 886-891). IEEE. DOI: 10.1109/CBMS58004.2023.00337
4	Another original contribution lies in the use of Faster R-CNN combined with a temporal layer in order to extract the spatial features of the aortic valve for a multi-frame problem. The resulted features are then used to detect the state of the aortic valve (open/closed) during an echocardiography sequence.	2.5.2.2, 2.5.2.3	Hatfaludi, C. A., Ciusdel, C. F., Toma, A., & Itu, L. M. (2022, September). Deep Learning based Aortic Valve Detection and State Classification on Echocardiographies. In **2022 IEEE 20th International Power Electronics and Motion Control Conference (PEMC)** (pp. 275-280). IEEE.
5	Another original contribution is using a model that was originally trained to predict the aortic valve as pretraining for a aortic stenosis detection model. We showed that the pretraining with freeze of weights, allowed the model to learn to detect aortic stenosis in an highly imbalanced dataset in which learning was not possible before.	2.6.3.2, 2.6.2	The results are not published.
6	Another original contribution is the use of multiple views as input for the model that detects the myocarditis. We analyzed how each view impact accuracy and we found the optimal view for the myocarditis detection.	3.2.2, 3.3	Hatfaludi, C.-A., Roșca, A., Popescu, A. B., Chitiboi, T., Sharma, P., Benedek, T., Itu, L. M. (2024). Automated Myocarditis Detection Using Deep Learning and MRI. **International Journal of Cardiovascular Imaging** - Under Review

7	Another original contribution for this study is the use of Few-Shot Learning in a multi-frame approach, where we combined a spatial CNN with a temporal CNN to detect the myocarditis for an highly imbalanced dataset. Even in this conditions, our model achieved an accuracy of 96.9%.	3.22	Hatfaludi, C.-A., Roșca, A., Popescu, A. B., Chitiboi, T., Sharma, P., Benedek, T., Itu, L. M. (2024). Automated Myocarditis Detection Using Deep Learning and MRI. **International Journal of Cardiovascular Imaging** - Under Review

6.3 Dissemination of Research Results

During the PhD program, the conducted research led to eight publications as author or co-author. Four journal articles were published as first author:

◘ Hatfaludi, C. A., Tache, I. A., Ciușdel, C. F., Puiu, A., Stoian, D., Itu, L. M., ...& Scafa-Udriste, A. (2022). Towards a Deep-Learning Approach for Prediction of Fractional Flow Reserve from Optical Coherence Tomography. Applied Sciences, 12(14), 6964 (impact factor: 2.7, Q2).

◘ Hatfaludi, C. A., Tache, I. A., Ciusdel, C. F., Puiu, A., Stoian, D., Calmac, L., ...& Itu, L. M. (2024). Co-registered optical coherence tomography and X-ray angiography for the prediction of fractional flow reserve. The International Journal of Cardiovascular Imaging, 1-11 (impact factor: 2.1, Q3).

◘ Hatfaludi, C. A., Danu, M. D., Leonte, H. A., Popescu, A. B., Condrea, F., Aldea, G. D., ...& Itu, L. M. (2023). Applications of Artificial Intelligence in Cardiovascular Emergencies–Status Quo and Outlook. Journal of Cardiovascular Emergencies, 9(4), 83-102 (impact factor: 0.6, Q4).

◘ Hatfaludi, C.-A., Roșca, A., Popescu, A. B., Chitiboi, T., Sharma, P., Benedek, T., Itu, L. M. (2024). Automated Myocarditis Detection Using Deep Learning and MRI. International Journal of Cardiovascular Imaging - Under Review.

Two journal articles were published as co-author:

◘ Tache, I. A., Hatfaludi, C. A., Puiu, A., Itu, L. M., Popa-Fotea, N. M., Calmac, L., & Scafa-Udriste, A. (2023). Assessment of the functional severity of coronary lesions from optical coherence tomography based on ensembled learning. BioMedical Engineering OnLine, 22(1), 127 (impact factor: 3.8, Q3).

◘ Popa-Fotea, N. M., Calmac, L., Micheu, M. M., Cosmin, M., Scarlatescu, A., Zamfir, D., ...& Scafa-Udriste, A. (2022). A cloud-based platform for clinical decision support in acute coronary syndrome patients: Study methodology. Kardiologia Polska (Polish Heart Journal), 80(5), 604-607 (impact factor: 3.7, Q2).

Two articles were published as first author in the proceedings of international conferences:

◘ Hatfaludi, C. A., Ciusdel, C. F., Toma, A., & Itu, L. M. (2022, September). Deep Learning based Aortic Valve Detection and State Classification on Echocardiographies. In 2022 IEEE 20th International Power Electronics and Motion Control Conference (PEMC) (pp. 275-280). IEEE.

◘ Hatfaludi, C. A., Bunescu, D., Ciuşdel, C. F., Serban, A., Böse, K., Oppel, M., ...& Itu, L. M. (2023, June). Deep learning based detection of collateral circulation in coronary angiographies. In 2023 IEEE 36th International Symposium on Computer-Based Medical Systems (CBMS) (pp. 886-891). IEEE.

6.4 Future Work

Directions for future work are described in the following:

- Expand Training Datasets: Aim to increase the training set sizes to boost the diagnostic performance of deep learning models, particularly for FFR prediction and myocarditis detection, while sourcing larger datasets to enhance model generalization across diverse patient populations.
- Enhance Input Data Complexity: Move towards using coronary lumen masks instead of the effective radius to account for lumen non-circularities, improving prediction accuracy, and explore incorporating 3D data inputs for capturing detailed anatomical features beyond the conventional 1D and 2D approaches.
- Develop Multi-Class Classification Models: Focus on creating models that can categorize lesions with greater precision, distinguishing between functionally significant, non-significant, and intermediate cases, to support nuanced clinical decisions and potentially reduce the need for invasive FFR measurements in ambiguous situations.
- Incorporate Additional Patient Information: Integrate comprehensive patient demographics and clinical data to refine diagnostic accuracy, and consider developing cascaded or hybrid models that utilize coronary and broader patient data for enhanced predictions.
- Adopt Advanced Deep Learning Techniques: Investigate the utility of graph neural networks and 3D data analysis models, along with self-supervised learning methods for pre-training on scarce annotated data, aiming to identify superior strategies for cardiac diagnosis.
- Automate Model Pre-training and Feature Extraction: Streamline the pre-training and feature extraction processes to minimize manual efforts, focusing on automating the detection of conditions like myocarditis and aortic stenosis with sophisticated feature extraction methods.
- Extend Models to Other Cardiac Conditions: Expand the disease detection models to cover a wider array of cardiac conditions and apply these models across different imaging modalities to assess adaptability and performance, thereby broadening the spectrum of detectable cardiac diseases.
- Validate Models in Multicenter Studies: Pursue extensive validation of the proposed deep learning models through multicenter studies, ensuring the inclusion of a diverse patient cohort to affirm the models' effectiveness and applicability in varied clinical environments.
- Explore Hemodynamic Quantities Prediction: Extend deep learning applications to predict critical hemodynamic quantities like CFR, rest Pd/Pa, iFR, and stenosis resistance under various conditions, enriching the diagnostic insights available to clinicians.

References

[1] K. Fukushima. "Neocognitron: A self-organizing neural network model for a mechanism of pattern recognition unaffected by shift in position". In: Biological cybernetics 36.4 (1980), pp. 193–202.

[2] S-C Lo et al. "Artificial convolution neural network techniques and applications for lung nodule detection". In: IEEE transactions on medical imaging 14.4 (1995), pp. 711–8.

[3] L Alzubaidi et al. "Review of deep learning: Concepts, CNN architectures, challenges, applications, future directions". In: Journal of big Data 8 (2021), pp. 1–74.

[4] X-X Yin et al. "U-Net-Based medical image segmentation". In: Journal of Healthcare Engineering 2022 (2022).

[5] J Collins, J Sohl-Dickstein, and D Sussillo. "Capacity and trainability in recurrent neural networks". In: arXiv preprint arXiv:161109913 (2016).

[6] R Grosse. Lecture 15: Exploding and vanishing gradients. University of Toronto Computer Science. 2017.

[7] MW Berry, A Mohamed, and BW Yap. Supervised and unsupervised learning for data science. Springer, 2019.

[8] M Moradi et al. "A cross-modality neural network transform for semi-automatic medical image annotation". In: Medical Image Computing and Computer-Assisted Intervention–MICCAI 2016: 19th International Conference, Athens, Greece, October 17-21, 2016, Proceedings, Part II. Springer. 2016, pp. 300–307.

[9] H Chen et al. "Iterative multi-domain regularized deep learning for anatomical structure detection and segmentation from ultrasound images". In: Medical Image Computing and Computer-Assisted Intervention–MICCAI 2016: 19th International Conference, Athens, Greece, October 17-21, 2016, Proceedings, Part II. Springer. 2016, pp. 487–495.

[10] G Carneiro, JC Nascimento, and A Freitas. "The segmentation of the left ventricle of the heart from ultrasound data using deep learning architectures and derivative-based search methods". In: IEEE Transactions on Image Processing 21.3 (2011), pp. 968–982.

[11] S Dong et al. "A combined fully convolutional networks and deformable model for automatic left ventricle segmentation based on 3D echocardiography". In: BioMed research international 2018 (2018).

[12] Florin C Ghesu et al. "Marginal space deep learning: efficient architecture for volumetric image parsing". In: IEEE transactions on medical imaging 35.5 (2016), pp. 1217–1228.

[13] Gerhard-Paul Diller et al. "Utility of machine learning algorithms in assessing patients with a systemic right ventricle". In: European Heart Journal-Cardiovascular Imaging 20.8 (2019), pp. 925–931.

[14] Tae Joon Jun et al. "Automated detection of vulnerable plaque in intravascular ultrasound images". In: Medical & Biological Engineering & Computing 57 (2019), pp. 863–876.

[15] J Zhang et al. "Fully automated echocardiogram interpretation in clinical practice: feasibility and diagnostic accuracy". In: Circulation 138.16 (2018), pp. 1623–1635.

[16] FT Dezaki et al. “Cardiac phase detection in echocardiograms with densely gated recurrent neural networks and global extrema loss”. In: IEEE transactions on medical imaging 38.8 (2018), pp. 1821–1832.

[17] AH Abdi et al. “Automatic quality assessment of echocardiograms using convolutional neural networks: feasibility on the apical four-chamber view”. In: IEEE transactions on medical imaging 36.6 (2017), pp. 1221–1230.

[18] F Commandeur et al. “Deep learning for quantification of epicardial and thoracic adipose tissue from non-contrast CT”. In: IEEE transactions on medical imaging 37.8 (2018), pp. 1835–1846.

[19] M Zreik et al. “Deep learning analysis of the myocardium in coronary CT angiography for identification of patients with functionally significant coronary artery stenosis”. In: Medical image analysis 44 (2018), pp. 72–85.

[20] D Wu et al. “Automated anatomical labeling of coronary arteries via bidirectional tree LSTMs”. In: International journal of computer assisted radiology and surgery 14 (2019), pp. 271–280.

[21] JM Wolterink et al. “Automatic coronary artery calcium scoring in cardiac CT angiography using paired convolutional neural networks”. In: Medical image analysis 34 (2016), pp. 123–136.

[22] N Lessmann et al. “Automatic calcium scoring in low-dose chest CT using deep neural networks with dilated convolutions”. In: IEEE transactions on medical imaging 37.2 (2017), pp. 615–625.

[23] W Bai et al. “Automated cardiovascular magnetic resonance image analysis with fully convolutional networks”. In: Journal of Cardiovascular Magnetic Resonance 20.1 (2018), pp. 1–12.

[24] H Yang et al. “Deep fusion net for multi-atlas segmentation: Application to cardiac MR images”. In: Medical Image Computing and Computer-Assisted Intervention–MICCAI 2016: 19th International Conference, Athens, Greece, October 17-21, 2016, Proceedings, Part II. Springer. 2016, pp. 521–528.

[25] H Yang et al. “Neural multi-atlas label fusion: Application to cardiac MR images”. In: Medical image analysis 49 (2018), pp. 60–75.

[26] MR Avendi, A Kheradvar, and H Jafarkhani. “A combined deep-learning and deformable-model approach to fully automatic segmentation of the left ventricle in cardiac MRI”. In: Medical image analysis 30 (2016), pp. 108–119.

[27] MR Avendi, A Kheradvar, and H Jafarkhani. “Automatic segmentation of the right ventricle from cardiac MRI using a learning-based approach”. In: Magnetic resonance in medicine 78.6 (2017), pp. 2439–2448.

[28] O Bernard et al. “Deep learning techniques for automatic MRI cardiac multi-structures segmentation and diagnosis: is the problem solved?” In: IEEE transactions on medical imaging 37.11 (2018), pp. 2514–2525.

[29] DM Vigneault et al. “ -net (omega-net): fully automatic, multi-view cardiac MR detection, orientation, and segmentation with deep neural networks”. In: Medical image analysis 48 (2018), pp. 95–106.

[30] Second Annual Data Science Bowl. Kaggle.

[31] G Luo et al. “Multi-views fusion CNN for left ventricular volumes estimation on cardiac MR images”. In: IEEE Transactions on Biomedical Engineering 65.9 (2017), pp. 1924–1934.

[32] F Liao et al. “Estimation of the volume of the left ventricle from MRI images using deep neural networks”. In: IEEE transactions on cybernetics 49.2 (2017), pp. 495–504.

[33] Q Dou et al. “3D deeply supervised network for automated segmentation of volumetric medical images”. In: Medical image analysis 41 (2017), pp. 40–54.

[34] S Moccia et al. “Development and testing of a deep learning-based strategy for scar segmentation on CMR-LGE images”. In: Magnetic Resonance Materials in Physics, Biology and Medicine 32 (2019), pp. 187–195.

[35] AS Fahmy et al. “Automated cardiac MR scar quantification in hypertrophic cardiomyopathy using deep convolutional neural networks”. In: JACC: Cardiovascular Imaging 11.12 (2018), pp. 1917–1918.

[36] C Xu et al. “Direct delineation of myocardial infarction without contrast agents using a joint motion feature learning architecture”. In: Medical image analysis 50 (2018), pp. 82–94.

[37] O Emad, IA Yassine, and AS Fahmy. “Automatic localization of the left ventricle in cardiac MRI images using deep learning”. In: 2015 37th Annual International Conference of the IEEE Engineering in Medicine and Biology Society (EMBC). IEEE. 2015, pp. 683–686.

[38] L Zhang et al. “Automatic assessment of full left ventricular coverage in cardiac cine magnetic resonance imaging with fisher-discriminative 3-D CNN”. In: IEEE Transactions on Biomedical Engineering 66.7 (2018), pp. 1975–1986.

[39] B Kong et al. “Recognizing end-diastole and end-systole frames via deep temporal regression network”. In: Medical Image Computing and Computer-Assisted Intervention-MICCAI 2016: 19th International Conference, Athens, Greece, October 17-21, 2016, Proceedings, Part III. Springer. 2016, pp. 264–272.

[40] F Yang et al. “Convolutional neural network for the detection of end-diastole and end-systole frames in free-breathing cardiac magnetic resonance imaging”. In: Computational and mathematical methods in medicine 2017 (2017).

[41] J Schlemper et al. “A deep cascade of convolutional neural networks for dynamic MR image reconstruction”. In: IEEE transactions on Medical Imaging 37.2 (2017), pp. 491–503.

[42] A Bratt et al. “Machine learning derived segmentation of phase velocity encoded cardiovascular magnetic resonance for fully automated aortic flow quantification”. In: Journal of Cardiovascular Magnetic Resonance 21 (2019), pp. 1–11.

[43] J Betancur et al. “Deep learning for prediction of obstructive disease from fast myocardial perfusion SPECT: a multicenter study”. In: JACC: Cardiovascular Imaging 11.11 (2018), pp. 1654–1663.

[44] J Betancur et al. “Deep learning analysis of upright-supine high-efficiency SPECT myocardial perfusion imaging for prediction of obstructive coronary artery disease: a multicenter study”. In: Journal of Nuclear Medicine 60.5 (2019), pp. 664–670.

[45] P Sadda and T Qarni. “Real-time medical video denoising with deep learning: application to angiography”. In: International journal of applied information systems 12.13 (2018), p. 22.

[46] K Breininger et al. “Intraoperative stent segmentation in X-ray fluoroscopy for endovascular aortic repair”. In: International journal of computer assisted radiology and surgery 13 (2018), pp. 1221–1231.

[47] D Toth et al. “3D/2D model-to-image registration by imitation learning for cardiac procedures”. In: International journal of computer assisted radiology and surgery 13 (2018), pp. 1141–1149.

[48] A Abdolmanafi et al. “Characterization of coronary artery pathological formations from OCT imaging using deep learning”. In: Biomedical optics express 9.10 (2018), pp. 4936–4960.

[49] N Gessert et al. “Automatic plaque detection in IVOCT pullbacks using convolutional neural networks”. In: IEEE transactions on medical imaging 38.2 (2018), pp. 426–434.

[50] M Kolossváry et al. “Cardiac computed tomography radiomics”. In: Journal of thoracic imaging 33.1 (2018), pp. 26–34.

[51] YL Yong et al. “Linear-regression convolutional neural network for fully automated coronary lumen segmentation in intravascular optical coherence tomography”. In: Journal of biomedical optics 22.12 (2017), p. 126005.

[52] AI Aviles-Rivero, SM Alsaleh, and A Casals. “Sliding to predict: vision-based beating heart motion estimation by modeling temporal interactions”. In: International Journal of Computer Assisted Radiology and Surgery 13 (2018), pp. 353–361.

[53] Vascular Disease: Types, Causes, Symptoms and Treatment. `https://my.clevelandclinic.org/health/diseases/17604-vascular-disease`. Accessed: 2024-02-15.

[54] Author details not provided. “Cardiovascular diseases for 10 causes, 1990 to 2015”. In: Journal of the American college of cardiology 70.1 (2017), pp. 1–25.

[55] E. Galkina and K. Ley. “Immune and inflammatory mechanisms of atherosclerosis”. In: Annual review of immunology 27 (2009).

[56] J. Erdmann et al. “A decade of genome-wide association studies for coronary artery disease: the challenges ahead”. In: Cardiovascular research 114.9 (2018), pp. 1241–1257.

[57] P. F. Teunissen, A. J. Horrevoets, and N. van Royen. “The coronary collateral circulation: genetic and environmental determinants in experimental models and humans”. In: Journal of molecular and cellular cardiology 52.4 (2012), pp. 897–904.

[58] N. van Royen et al. “A critical review of clinical arteriogenesis research”. In: Journal of the American College of Cardiology 55.1 (2009), pp. 17–25.

[59] T. Pohl et al. “Frequency distribution of collateral flow and factors influencing collateral channel development: functional collateral channel measurement in 450 patients with coronary artery disease”. In: Journal of the American College of Cardiology 38.7 (2001), pp. 1872–1878.

[60] S. Schirmer et al. “Stimulation of collateral artery growth: travelling further down the road to clinical application”. In: Heart 95.3 (2009), pp. 191–197.

[61] G.-H. Choo. “Collateral circulation in chronic total occlusions–an interventional perspective”. In: Current Cardiology Reviews 11.4 (2015), pp. 277–284.

[62] P. Meier et al. “Beneficial effect of recruitable collaterals: a 10-year follow-up study in patients with stable coronary artery disease undergoing quantitative collateral measurements”. In: Circulation 116.9 (2007), pp. 975–983.

[63] P. Meier et al. “The impact of the coronary collateral circulation on mortality: a meta-analysis”. In: European heart journal 33.5 (2012), pp. 614–621.

[64] W. Schaper. “Collateral vessels reduce mortality”. In: European heart journal 33 (2012), pp. 564–566.

[65] B. Wang et al. “Coronary collateral circulation: Effects on outcomes of acute anterior myocardial infarction after primary percutaneous coronary intervention”. In: Journal of geriatric cardiology: JGC 8.2 (2011), p. 93.

[66] L. Liu et al. “Automatic assessment of collateral physiology in chronic total occlusions by means of artificial intelligence”. In: Cardiol. J (2022).

[67] H. Kuang et al. “Automated Collateral Scoring on CT Angiography of Patients with Acute Ischemic Stroke Using Hybrid CNN and Transformer Network”. In: Biomedicines 11.2 (2023), p. 243.

[68] L. Wolff et al. “Diagnostic performance of an algorithm for automated collateral scoring on computed tomography angiography”. In: European radiology 32.8 (2022), pp. 5711–5718.

[69] M. Aktar et al. “Deep learning for collateral evaluation in ischemic stroke with imbalanced data”. In: International Journal of Computer Assisted Radiology and Surgery (2023), pp. 1–8.

[70] K. Iyer et al. "Angionet: a convolutional neural network for vessel segmentation in X-ray angiography". In: Scientific Reports 11.1 (2021), p. 18066.

[71] S. G. van Velzen et al. "Deep learning for automatic calcium scoring in CT: validation using multiple cardiac CT and chest CT protocols". In: Radiology 295.1 (2020), pp. 66–79.

[72] G. Li et al. "Prediction of 3D Cardiovascular hemodynamics before and after coronary artery bypass surgery via deep learning". In: Communications biology 4.1 (), p. 99.

[73] Centers for Disease Control and Prevention (CDC). Valvular Heart Disease. https://www.cdc.gov/heartdisease/valvular_disease.htm. Accessed: 2024-02-15.

[74] National Heart, Lung, and Blood Institute (NHLBI), NIH. Heart Valve Diseases - Types. https://www.nhlbi.nih.gov/health-topics/heart-valve-diseases. Accessed: 2024-02-15.

[75] Matthew J Czarny and Jon R Resar. "Diagnosis and management of valvular aortic stenosis". In: Clinical Medicine Insights: Cardiology 8 (2014), CMC–S15716.

[76] Stefania Sacchi et al. "Doppler assessment of aortic stenosis: a 25-operator study demonstrating why reading the peak velocity is superior to velocity time integral". In: European Heart Journal-Cardiovascular Imaging 19.12 (2018), pp. 1380–1389.

[77] P. Généreux et al. "Staging classification of aortic stenosis based on the extent of cardiac damage". In: European heart journal 38.45 (2017), pp. 3351–3358.

[78] M. Berthelot-Richer et al. "Discordant grading of aortic stenosis severity: echocardiographic predictors of survival benefit associated with aortic valve replacement". In: JACC: Cardiovascular Imaging 9.7 (2016), pp. 797–805.

[79] H. Baumgartner et al. "Echocardiographic assessment of valve stenosis: EAE/ASE recommendations for clinical practice". In: Journal of the American Society of Echocardiography 22.1 (2009), pp. 1–23.

[80] J. Zhang et al. "Fully automated echocardiogram interpretation in clinical practice: feasibility and diagnostic accuracy". In: Circulation 138.16 (2018), pp. 1623–1635.

[81] A. Madani et al. "Fast and accurate view classification of echocardiograms using deep learning". In: NPJ digital medicine 1.1 (2018), pp. 1–8.

[82] A. Narang et al. "Machine learning based automated dynamic quantification of left heart chamber volumes". In: European Heart Journal-Cardiovascular Imaging 20.5 (2019), pp. 541–549.

[83] V. Volpato et al. "Automated, machine learning based, 3D echocardiographic quantification of left ventricular mass". In: Echocardiography 36.2 (2019), pp. 312–319.

[84] Benjamin Seth Wessler, Duo Huang, and Gary Long Jr. "IDENTIFICATION OF SEVERE AORTIC STENOSIS USING DEEP LEARNING". In: Journal of the American College of Cardiology 75.11_Supplement_1 (2020), pp. 3493–3493.

[85] Heart Inflammation: Causes, Symptoms and Treatments. https://my.clevelandclinic.org/health/diseases/23052-heart-inflammation. Accessed: 2024-02-15.

[86] S. Sagar, P. P. Liu, and L. T. Cooper. "Myocarditis". In: The Lancet 379.9817 (2012), pp. 738–747.

[87] V. Kytö et al. "Diagnosis and presentation of fatal myocarditis". In: Human pathology 36.9 (2005), pp. 1003–1007.

[88] D. Sharifrazi et al. CNN-KCL: Automatic myocarditis diagnosis using convolutional neural network combined with k-means clustering. 2020.

[89] A. Asher. "A review of endomyocardial biopsy and current practice in England: out of date or underutilised". In: Br J Cardiol 24.3 (2017), pp. 108–112.

[90] M. P. Gannon et al. “State of the art: Evaluation and prognostication of myocarditis using cardiac MRI”. In: Journal of Magnetic Resonance Imaging 49.7 (2019), e122–e131.

[91] M. Abdar et al. “Performance improvement of decision trees for diagnosis of coronary artery disease using multi filtering approach”. In: 2019 IEEE 4th International Conference on Computer and Communication Systems (ICCCS). IEEE. 2019, pp. 26–30.

[92] Y. Wang et al. “Generalizing from a few examples: A survey on few-shot learning”. In: ACM computing surveys (csur) 53.3 (2020), pp. 1–34.

[93] A. Shoeibi et al. “Automatic diagnosis of myocarditis in cardiac magnetic images using CycleGAN and deep PreTrained models”. In: International work-conference on the interplay between natural and artificial computation. Springer, 2022, pp. 145–155.

[94] Thomas J Ryan. “The coronary angiogram and its seminal contributions to cardiovascular medicine over five decades”. In: Circulation 106.6 (2002), pp. 752–756.

[95] Juan Luis Gutierrez-Chico et al. “Optical coherence tomography: from research to practice”. In: European Heart Journal–Cardiovascular Imaging 13.5 (2012), pp. 370–384.

[96] Juan Luis Gutiérrez-Chico et al. “Delayed coverage in malapposed and side-branch struts with respect to well-apposed struts in drug-eluting stents: in vivo assessment with optical coherence tomography”. In: Circulation 124.5 (2011), pp. 612–623.

[97] Juan Luis Gutiérrez-Chico et al. “Vascular tissue reaction to acute malapposition in human coronary arteries: sequential assessment with optical coherence tomography”. In: Circulation: Cardiovascular Interventions 5.1 (2012), pp. 20–29.

[98] Ziad A Ali et al. “Optical coherence tomography compared with intravascular ultrasound and with angiography to guide coronary stent implantation (ILUMIEN III: OPTIMIZE PCI): a randomised controlled trial”. In: The Lancet 388.10060 (2016), pp. 2618–2628.

[99] N. Gonzalo et al. “Morphometric assessment of coronary stenosis relevance with optical coherence tomography: a comparison with fractional flow reserve and intravascular ultrasound”. In: Journal of the American College of Cardiology 59 (2012), pp. 1080–1089.

[100] N.H. Pijls et al. “Measurement of fractional flow reserve to assess the functional severity of coronary-artery stenoses”. In: New England Journal of Medicine 334 (1996), pp. 1703–1708.

[101] P.A. Tonino et al. “Fractional flow reserve versus angiography for guiding percutaneous coronary intervention”. In: New England Journal of Medicine 360 (2009), pp. 213–224.

[102] S. Tu et al. “Image-based assessment of fractional flow reserve”. In: EuroIntervention: journal of EuroPCR in collaboration with the Working Group on Interventional Cardiology of the European Society of Cardiology 11 (2015), pp. V50–54.

[103] D.H. Yang et al. “Diagnostic performance of on-site CT-derived fractional flow reserve versus CT perfusion”. In: European Heart Journal–Cardiovascular Imaging 18 (2017), pp. 432–440.

[104] A. Coenen et al. “Fractional flow reserve computed from noninvasive CT angiography data: diagnostic performance of an on-site clinician-operated computational fluid dynamics algorithm”. In: Radiology 274 (2015), pp. 674–683.

[105] M. Renker et al. “Comparison of diagnostic value of a novel noninvasive coronary computed tomography angiography method versus standard coronary angiography for assessing fractional flow reserve”. In: The American Journal of Cardiology 114 (2014), pp. 1303–1308.

[106] B.-K. Koo et al. “Diagnosis of ischemia-causing coronary stenoses by noninvasive fractional flow reserve computed from coronary computed tomographic angiograms: results from the prospective multicenter DISCOVER-FLOW study”. In: Journal of the American College of Cardiology 58 (2011), pp. 1989–1997.

[107] S. Tu et al. "Diagnostic accuracy of fast computational approaches to derive fractional flow reserve from diagnostic coronary angiography: the international multicenter FAVOR pilot study". In: Cardiovascular Interventions 9 (2016), pp. 2024–2035.

[108] M. Tröbs et al. "Comparison of fractional flow reserve based on computational fluid dynamics modeling using coronary angiographic vessel morphology versus invasively measured fractional flow reserve". In: The American Journal of Cardiology 117 (2016), pp. 29–35.

[109] M.I. Papafaklis et al. "Fast virtual functional assessment of intermediate coronary lesions using routine angiographic data and blood flow simulation in humans: comparison with pressure wire-fractional flow reserve". In: EuroIntervention 10 (2014), pp. 574–583.

[110] S. Tu et al. "Fractional flow reserve calculation from 3-dimensional quantitative coronary angiography and TIMI frame count: a fast computer model to quantify the functional significance of moderately obstructed coronary arteries". In: JACC: Cardiovascular Interventions 7 (2014), pp. 768–777.

[111] P.D. Morris et al. "Virtual fractional flow reserve from coronary angiography: modeling the significance of coronary lesions: results from the VIRTU-1 study". In: JACC: Cardiovascular Interventions 6 (2013), pp. 149–157.

[112] F. Seike et al. "Intracoronary optical coherence tomography-derived virtual fractional flow reserve for the assessment of coronary artery disease". In: The American Journal of Cardiology 120 (2017), pp. 1772–1779.

[113] S.-J. Jang et al. "Comparison of accuracy of one-use methods for calculating fractional flow reserve by intravascular optical coherence tomography to that determined by the pressure-wire method". In: The American Journal of Cardiology 120 (2017), pp. 1920–1925.

[114] W. Yu et al. "Diagnostic accuracy of intracoronary optical coherence tomography-derived fractional flow reserve for assessment of coronary stenosis severity". In: EuroIntervention: journal of EuroPCR in collaboration with the Working Group on Interventional Cardiology of the European Society of Cardiology 15 (2019), p. 189.

[115] J. Ha et al. "Assessing computational fractional flow reserve from optical coherence tomography in patients with intermediate coronary stenosis in the left anterior descending artery". In: Circulation: Cardiovascular Interventions 9 (2016), e003613.

[116] L. Itu et al. "A patient-specific reduced-order model for coronary circulation". In: Proceedings of the 2012 9th IEEE International Symposium on Biomedical Imaging (ISBI). 2012, pp. 832–835.

[117] S.-B. Deng et al. "Diagnostic performance of noninvasive fractional flow reserve derived from coronary computed tomography angiography in coronary artery disease: a systematic review and meta-analysis". In: International Journal of Cardiology 184 (2015), pp. 703–709.

[118] C.M. Bishop and N.M. Nasrabadi. Pattern Recognition and Machine Learning. Vol. 4. Springer, 2006.

[119] Y. Zheng and D. Comaniciu. "Marginal space learning for medical image analysis". In: Springer 2.6 (2014).

[120] T. Mansi et al. "Data-driven reduction of a cardiac myofilament model". In: Proceedings of the International Conference on Functional Imaging and Modeling of the Heart. 2013, pp. 232–240.

[121] K. Tøndel et al. "Hierarchical Cluster-based Partial Least Squares Regression (HC-PLSR) is an efficient tool for metamodelling of nonlinear dynamic models". In: BMC Systems Biology 5 (2011), pp. 1–17.

[122] L. Itu et al. "A machine-learning approach for computation of fractional flow reserve from coronary computed tomography". In: Journal of Applied Physiology 121 (2016), pp. 42–52.

[123] H. Cho et al. "Angiography based machine learning for predicting fractional flow reserve in intermediate coronary artery lesions". In: Journal of the American Heart Association 8 (2019), e011685.

[124] J.-J. Cha et al. "Optical coherence tomography-based machine learning for predicting fractional flow reserve in intermediate coronary stenosis: a feasibility study". In: Scientific Reports 10 (2020), pp. 1–8.

[125] J.-G. Lee et al. "Intravascular ultrasound-based machine learning for predicting fractional flow reserve in intermediate coronary artery lesions". In: Atherosclerosis 292 (2020), pp. 171–177.

[126] L. Deng and D. Yu. "Deep learning: methods and applications". In: Foundations and Trends in Signal Processing 7 (2014), pp. 197–387.

[127] Y. LeCun, Y. Bengio, and G. Hinton. "Deep learning". In: Nature 521 (2015), pp. 436–444.

[128] Y. Wang et al. "Generalizing from a few examples: A survey on few-shot learning". In: ACM Computing Surveys (CSUR) 53 (2020), pp. 1–34.

[129] X. Jiang et al. "Automatic detection of coronary metallic stent struts based on YOLOv3 and R-FCN". In: Computational and Mathematical Methods in Medicine (2020).

[130] Z. Wang et al. "3-D stent detection in intravascular OCT using a Bayesian network and graph search". In: IEEE Transactions on Medical Imaging 34 (2015), pp. 1549–1561.

[131] P. Wu et al. "Automatic stent reconstruction in optical coherence tomography based on a deep convolutional model". In: Biomedical Optics Express 11 (2020), pp. 3374–3394.

[132] G. Yang et al. "Stent detection with very thick tissue coverage in intravascular OCT". In: Biomedical Optics Express 12 (2021), pp. 7500–7516.

[133] Yu Shi Lau et al. "Automated segmentation of metal stent and bioresorbable vascular scaffold in intravascular optical coherence tomography images using deep learning architectures". In: Physics in Medicine & Biology 66.24 (2021), p. 245026.

[134] J. Lee et al. "Segmentation of Coronary Calcified Plaque in Intravascular OCT Images Using a Two-Step Deep Learning Approach". In: IEEE Access 8 (2020), pp. 225581–225593.

[135] Y. Gharaibeh et al. "Coronary calcification segmentation in intravascular OCT images using deep learning: application to calcification scoring". In: Journal of Medical Imaging 6 (2019), p. 045002.

[136] A. Abdolmanafi et al. "A deep learning based model for characterization of atherosclerotic plaque in coronary arteries using optical coherence tomography images". In: Medical Physics 48 (2021), pp. 3511–3524.

[137] Elżbieta Pociask et al. "Fully automated lumen segmentation method for intracoronary optical coherence tomography". In: Journal of Healthcare Engineering 2018 (2018).

[138] C. Jiao et al. "Machine learning classification of origins and varieties of Tetrastigma hemsleyanum using a dual-mode microscopic hyperspectral imager". In: Spectrochimica Acta Part A: Molecular and Biomolecular Spectroscopy 261 (2021), p. 120054.

[139] T. Wang et al. "Smartphone imaging spectrometer for egg/meat freshness monitoring". In: Analytical Methods 14 (2022), pp. 508–517.

[140] J. Snell, K. Swersky, and R. Zemel. "Prototypical networks for few-shot learning". In: 30 ().

[141] M.J. Kern et al. "Physiological assessment of coronary artery disease in the cardiac catheterization laboratory: a scientific statement from the American Heart Association Committee on Diagnostic and Interventional Cardiac Catheterization, Council on Clinical Cardiology". In: Circulation 114 (2006), pp. 1321–1341.

[142] G. Bradski. "The openCV library". In: Dr. Dobb's Journal: Software Tools for the Professional Programmer 25 (2000), pp. 120–123.

[143] S. Patro and K.K. Sahu. “Normalization: A preprocessing stage”. In: arXiv preprint arXiv:1503.06462 (2015).

[144] A.F. Agarap. “Deep learning using rectified linear units (relu)”. In: arXiv preprint arXiv:1803.08375 (2018).

[145] S. Santurkar et al. “How does batch normalization help optimization?” In: 31 ().

[146] R. Dey and F.M. Salem. “Gate-variants of gated recurrent unit (GRU) neural networks”. In: Proceedings of the 2017 IEEE 60th international midwest symposium on circuits and systems (MWSCAS). 2017, pp. 1597–1600.

[147] J. Han and C. Moraga. “The influence of the sigmoid function parameters on the speed of backpropagation learning”. In: Proceedings of the International workshop on artificial neural networks. 1995, pp. 195–201.

[148] T.-T. Wong. “Performance evaluation of classification algorithms by k-fold and leave-one-out cross validation”. In: Pattern Recognition 48 (2015), pp. 2839–2846.

[149] Z. Zhang. “Improved adam optimizer for deep neural networks”. In: Proceedings of the 2018 IEEE/ACM 26th International Symposium on Quality of Service (IWQoS). 2018, pp. 1–2.

[150] Douglas M Kline and Victor L Berardi. “Revisiting squared-error and cross-entropy functions for training neural network classifiers”. In: Neural Computing & Applications 14 (2005), pp. 310–318.

[151] P. Liashchynskyi and P. Liashchynskyi. “Grid search, random search, genetic algorithm: A big comparison for NAS”. In: arXiv preprint arXiv:1912.06059 (2019).

[152] A. Paszke et al. “Pytorch: An imperative style, high-performance deep learning library”. In: 32 ().

[153] Z.H. Hoo, J. Candlish, and D. Teare. “What is an ROC curve?” In: 2017 34 (), pp. 357–359.

[154] J.M. Lobo, A. Jiménez Valverde, and R. Real. “AUC: a misleading measure of the performance of predictive distribution models”. In: Global Ecology and Biogeography 17 (2008), pp. 145–151.

[155] I. Unal. “Defining an optimal cut-point value in ROC analysis: an alternative approach”. In: Computational and Mathematical Methods in Medicine 2017 (2017).

[156] W.J. Youden. “Index for rating diagnostic tests”. In: Cancer 3 (1950), pp. 32–35.

[157] H.B. Wong and G.H. Lim. “Measures of diagnostic accuracy: sensitivity, specificity, PPV and NPV”. In: Proceedings of Singapore Healthcare 20 (2011), pp. 316–318.

[158] T.S. Genders et al. “Methods for calculating sensitivity and specificity of clustered data: a tutorial”. In: Radiology 265 (2012), pp. 910–916.

[159] B. Lakshminarayanan, A. Pritzel, and C. Blundell. “Simple and scalable predictive uncertainty estimation using deep ensembles”. In: Advances in Neural Information Processing Systems 2017. Vol. 30.

[160] Luis Bote-Curiel et al. “Deep learning and big data in healthcare: a double review for critical beginners”. In: Applied Sciences 9.11 (2019), p. 2331.

[161] O. Demir-Kavuk et al. “Prediction using step-wise L1, L2 regularization and feature selection for small data sets with a large number of features”. In: BMC Bioinformatics 12 (2011), pp. 1–10.

[162] N. Srivastava et al. “Dropout: A simple way to prevent neural networks from overfitting”. In: The Journal of Machine Learning Research 15 (2014), pp. 1929–1958.

[163] S.C. Wong et al. “Understanding data augmentation for classification: When to warp?” In: Proceedings of the 2016 International Conference on Digital Image Computing: Techniques and Applications (DICTA). 2016, pp. 1–6.

[164] K.K. Kumamaru et al. "Diagnostic accuracy of 3D deep-learning-based fully automated estimation of patient-level minimum fractional flow reserve from coronary computed tomography angiography". In: European Heart Journal-Cardiovascular Imaging 21 (2020), pp. 437–445.

[165] M. Zreik et al. "Deep learning analysis of coronary arteries in cardiac CT angiography for detection of patients requiring invasive coronary angiography". In: IEEE Transactions on Medical Imaging 39 (2019), pp. 1545–1557.

[166] Y. Wang et al. "Generalizing from a few examples: A survey on few-shot learning". In: ACM computing surveys (csur) 53.3 (2020), pp. 1–34.

[167] J. Snell, K. Swersky, and R. Zemel. "Prototypical networks for few-shot learning". In: Advances in neural information processing systems. Vol. 30. 2017.

[168] K. P. Rentrop et al. "Changes in collateral channel filling immediately after controlled coronary artery occlusion by an angioplasty balloon in human subjects". In: Journal of the American College of Cardiology 5.3 (1985), pp. 587–592.

[169] D. C. Levin. "Pathways and functional significance of the coronary collateral circulation". In: Circulation 50.4 (1974), pp. 831–837.

[170] M. Tayebjee, G. Lip, and R. MacFadyen. "Collateralization and the response to obstruction of epicardial coronary arteries". In: Qjm 97.5 (2004), pp. 259–272.

[171] C. M. Gibson et al. "Angiographic methods to assess human coronary angiogenesis". In: American heart journal 137.1 (1999), pp. 169–179.

[172] C. Cheadle et al. "Analysis of microarray data using Z score transformation". In: The Journal of molecular diagnostics 5.2 (2003), pp. 73–81.

[173] X. Yin et al. "A flexible sigmoid function of determinate growth". In: Annals of botany 91.3 (2003), pp. 361–371.

[174] T. Fushiki. "Estimation of prediction error by using K-fold cross-validation". In: Statistics and Computing 21 (2011), pp. 137–146.

[175] Z. Zhang. "Improved adam optimizer for deep neural networks". In: 2018 IEEE/ACM 26th international symposium on quality of service (IWQoS). IEEE, 2018, pp. 1–2.

[176] K. Simonyan, A. Vedaldi, and A. Zisserman. Deep inside convolutional networks: Visualising image classification models and saliency maps. arXiv preprint arXiv:13126034. 2013.

[177] H. B. Wong and G. H. Lim. "Measures of diagnostic accuracy: sensitivity, specificity, PPV and NPV". In: Proceedings of Singapore healthcare 20.4 (2011), pp. 316–318.

[178] F. C. Ghesu et al. "Contrastive self-supervised learning from 100 million medical images with optional supervision". In: Journal of Medical Imaging 9.6 (2022), p. 064503.

[179] L. Deng and D. Yu. "Deep learning: methods and applications". In: Foundations and trends in signal processing 7.3–4 (2014), pp. 197–387.

[180] A. Krizhevsky, I. Sutskever, and G. E. Hinton. "Imagenet classification with deep convolutional neural networks". In: Advances in neural information processing systems. Vol. 25. 2012.

[181] K. Simonyan and A. Zisserman. "Very deep convolutional networks for large-scale image recognition". In: arXiv preprint arXiv:1409.1556 (2014).

[182] K. He et al. "Deep residual learning for image recognition". In: Proceedings of the IEEE conference on computer vision and pattern recognition. 2016, pp. 770–778.

[183] J. Redmon and A. Farhadi. "Yolov3: An incremental improvement". In: arXiv preprint arXiv:1804.02767 (2018).

[184] S. Ren et al. "Faster r-cnn: Towards real-time object detection with region proposal networks". In: Advances in neural information processing systems. Vol. 28. 2015.

[185] R. Girshick et al. “Rich feature hierarchies for accurate object detection and semantic segmentation”. In: Proceedings of the IEEE conference on computer vision and pattern recognition. 2014, pp. 580–587.

[186] Z. Zhang. “Improved adam optimizer for deep neural networks”. In: 2018 IEEE/ACM 26th International Symposium on Quality of Service (IWQoS). IEEE, 2018, pp. 1–2.

[187] C. Cheadle et al. “Analysis of microarray data using Z score transformation”. In: The Journal of molecular diagnostics 5.2 (2003), pp. 73–81.

[188] Tadayoshi Fushiki. “Estimation of prediction error by using K-fold cross-validation”. In: Statistics and Computing 21 (2011), pp. 137–146.

[189] M. Buckland and F. Gey. “The relationship between recall and precision”. In: Journal of the American society for information science 45.1 (1994), pp. 12–19.

[190] H. Rezatofighi et al. “Generalized intersection over union: A metric and a loss for bounding box regression”. In: Proceedings of the IEEE/CVF conference on computer vision and pattern recognition. 2019, pp. 658–666.

[191] K. W. Lai et al. “Detection of Aortic Valve Using Deep Learning Approaches”. In: 2020 IEEE-EMBS Conference on Biomedical Engineering and Sciences (IECBES). IEEE, 2021, pp. 538–542.

[192] M. H. bin Ahmad Nizar et al. “Detection of aortic valve from echocardiography in real-time using convolutional neural network”. In: 2018 IEEE-EMBS Conference on Biomedical Engineering and Sciences (IECBES). IEEE, 2018, pp. 91–95.

[193] J. M. Kwon et al. “Deep learning–based algorithm for detecting aortic stenosis using electrocardiography”. In: Journal of the American Heart Association 9.7 (2020).

[194] G. Katti, S. A. Ara, and A. Shireen. “Magnetic resonance imaging (MRI)–A review”. In: International journal of dental clinics 3.1 (2011), pp. 65–70.

[195] L. Deng and D. Yu. “Deep learning: methods and applications”. In: Foundations and trends in signal processing 7.3–4 (2014), pp. 197–387.

[196] S. V. Moravvej et al. “RLMD-PA: A reinforcement learning-based myocarditis diagnosis combined with a population-based algorithm for pretraining weights”. In: Contrast Media & Molecular Imaging 2022 (2022).

[197] S. Patro and K. K. Sahu. Normalization: A preprocessing stage. arXiv preprint arXiv:150306462. 2015.

[198] X. Zeng, D. F. Wong, and L. S. Chao. “Constructing better classifier ensemble based on weighted accuracy and diversity measure”. In: The Scientific World Journal 2014 (2014).

[199] Z. H. Hoo, J. Candlish, and D. Teare. What is an ROC curve? BMJ Publishing Group Ltd and the British Association for Accident … 2017.

[200] J. M. Lobo, A. Jiménez Valverde, and R. Real. “AUC: a misleading measure of the performance of predictive distribution models”. In: Global ecology and Biogeography 17.2 (2008), pp. 145–151.

[201] I. Unal. “Defining an optimal cut-point value in ROC analysis: an alternative approach”. In: Computational and mathematical methods in medicine 2017 (2017).

[202] H. B. Wong and G. H. Lim. “Measures of diagnostic accuracy: sensitivity, specificity, PPV and NPV”. In: Proceedings of Singapore healthcare 20.4 (2011), pp. 316–318.

[203] W. J. Youden. “Index for rating diagnostic tests”. In: Cancer 3.1 (1950), pp. 32–35.

[204] R. Kumari and S. K. Srivastava. “Machine learning: A review on binary classification”. In: International Journal of Computer Applications 160.7 (2017).

[205] H. Pratiwi et al. “Sigmoid activation function in selecting the best model of artificial neural networks”. In: Journal of Physics: Conference Series. Vol. 012010. IOP Publishing, 2020.

[206] T. Fushiki. “Estimation of prediction error by using K-fold cross-validation”. In: Statistics and Computing 21 (2011), pp. 137–146.

[207] Y. Zhang et al. “Design and Demonstration of (AlxGal-x) 2 O 3/Ga 2 O 3 Double Heterostructure Field Effect Transistor (DHFET)”. In: 76th Device Research Conference (DRC). IEEE. 2018, pp. 1–2.

Abstract

In exploring the cutting-edge application of deep neural networks (DNNs) within cardiac healthcare, this thesis delves into the transformative potential these technologies hold for diagnosing a range of heart diseases, with a particular focus on vascular, valvular, and inflammatory conditions such as coronary artery disease, aortic stenosis, and myocarditis. Based on advanced medical imaging techniques, the research aims to bridge the gap between traditional diagnostic methods and the complex analysis capabilities afforded by DNNs, promising a significant leap in both the accuracy and early detection of cardiac pathologies.

Structured into comprehensive sections, the thesis first lays the groundwork by highlighting the global impact of cardiac diseases and the emerging role of DNNs in revolutionizing diagnostic processes. It then navigates through the intricacies of various DNN architectures, including convolutional and recurrent neural networks, underscoring their utility in dissecting and interpreting complex medical imagery.

Focusing on specific cardiac ailments, the research presents in-depth studies on the detection and analysis of vascular diseases through the identification of coronary collateral circulation using DNNs. It further investigates the applicability of these neural networks in diagnosing valvular heart diseases, with an emphasis on aortic stenosis, and extends the exploration to inflammatory cardiac conditions, showcasing myocarditis as a case study.

The thesis finally also synthesizes the insights gathered from these investigations, offering a comprehensive summary of the findings. It highlights the significant strides made towards integrating DNN technology into cardiac diagnostics, emphasizing the potential for enhancing the precision and timeliness of disease identification. Additionally, the conclusion points towards future research directions, suggesting a roadmap for further advancements in leveraging deep learning for cardiac health.

By connecting traditional diagnostic approaches with the sophisticated analytical capabilities of DNNs, this study not only lays the groundwork for enhanced precision and earlier detection of diseases but also unveils new horizons in tailored patient care, signaling the start of a new chapter in how we diagnose heart diseases.